TÉCNICO LISBOA

Influence of graft positioning on shoulder stability and articular contact pressure during the Latarjet Procedure

Rita Isabel Rosado Martins

Thesis to obtain the Master of Science Degree in

Biomedical Engineering

Supervisor(s): Prof. Carlos Miguel Fernandes Quental
Dra. Clara Isabel de Campos Azevedo

Examination Committee

Chairperson: Prof. Fernando Manuel Fernandes Simões
Supervisor: Prof. Carlos Miguel Fernandes Quental
Member of the Committee: Dra. Ana Catarina Leiria Pires Gago Ângelo
Prof. Luís Alberto Gonçalves de Sousa

November 2021

Declaration

I declare that this document is an original work of my own authorship and that it fulfills all the requirements of the Code of Conduct and Good Practices of the Universidade de Lisboa.

Preface

The work presented in this thesis was performed at Departamento de Engenharia Mecânica of Instituto Superior Técnico (Lisbon, Portugal), during the period February-October 2021, under the supervision of Prof. Carlos Quental. The thesis was co-supervised by Dr. Clara Azevedo.

Agradecimentos

Ao professor Carlos Quental e ao professor João Folgado, agradeço a enorme disponibilidade, o constante encorajamento, apoio e inúmeros conselhos que me mostraram durante este percurso. Gostaria também de agradecer à Dra. Carla Azevedo por todo interesse demonstrado e pela ajuda ao providenciar conhecimentos médicos essenciais.

Agradeço também à minha família que, longe ou perto, me deram apoio incondicional durante todas as fases da vida. Um agradecimento especial ao meu irmão pelas respostas às minhas mais variadas dúvidas.

Finalmente, aos meus amigos, obrigada por todos os incentivos não só durante estes meses, mas durante anos. Obrigada pela imensa companhia, boa-disposição e pelas simples mensagens que me motivaram mais do que qualquer possível recompensa.

Resumo

O procedimento de Latarjet é o procedimento cirúrgico mais utilizado para tratar pacientes com instabilidade anterior do ombro na presença de grandes defeitos ósseos na glenóide. Apesar da posição do enxerto ósseo afetar significativamente a eficácia deste procedimento, a faixa de posições aceite para o seu posicionamento apropriado ainda é alvo de discussão. Desta forma, o principal objetivo do estudo é avaliar o posicionamento ótimo do enxerto ósseo durante o procedimento de Latarjet, fazendo um balanço entre a restauração da estabilidade da articulação e o risco de osteoartrite. Para realizar isto, quatro modelos de elementos finitos da articulação do ombro após o procedimento de Latarjet foram desenvolvidos ao variar a posiçáo do enxerto na direção medial-lateral. Para cada posição do enxerto, quatro posições do ombro foram modeladas. Uma força compressiva e uma translação anterior foram aplicadas simultaneamente à cabeça humeral para permitir a análise do rácio de estabilidade e da distribuição de pressões de contacto da articulação glenohumeral. A posição ideal to enxerto foi determinada como sendo entre 1,81 mm na direção medial e 0,44 mm na direção lateral relativamente à superfície articular da glenóide numa vista axial. Enxertos colocados medialmente à superfície articular não contribuem para restaurar a estabilidade da articulação, enquanto que enxertos colocados lateralmente aumentam a pressão de contact acima da tensão de cedência da cartilagem.

Palavras-chave: Procedimento de Latarjet; Enxerto do coracóide; Modelo de elementos finitos; Instabilidade do ombro.

Abstract

The Latarjet procedure is the most popular surgical procedure used to treat anterior shoulder instability in the presence of large glenoid bone defects. Although the position of the bone graft largely affects the efficacy of this procedure, the accepted range for its proper positioning is still discussed. Thus, the main goal of this study is to assess the optimal positioning of the bone graft during the Latarjet procedure, by balancing both the restoration of joint stability and osteoarthritis risk. To accomplish this, four finite element models of the shoulder joint after the Latarjet procedure were developed by varying graft position in the medial-lateral direction. For each graft position, four arm positions were modeled. A compressive force and anterior translation were simultaneously applied to the humeral head for analysis of the glenohumeral joint stability ratio and contact pressure distribution. The optimal graft position was found to be between 1.81 mm medial and 0.44 mm lateral to the articular glenoid surface in an axial view. Grafts placed medial to the articular surface do not contribute to the restoration of joint stability, while grafts placed laterally increase contact pressures beyond the failure stress of cartilage.

Keywords: Latarjet Procedure; Coracoid graft; Finite Element model; Shoulder Instability.

Contents

List of Tables

List of Figures

List of Abreviations

3D Three dimensional

AC Acromioclavicular

CT Computed Tomography

FE Finite Element

GH Glenohumeral

ROM Range of Motion

SC Sternoclavicular

SR Stability Ratio

STL Sterolithography

ST Scapulothoracic

Chapter 1

Introduction

1.1 Motivation and Objectives

The glenohumeral joint is one of the joints that makes up the shoulder articular complex, possessing the largest range of motion of all the joints in the human body. Its high mobility is associated with the incongruity of the articular faces, which leads to a sacrifice in joint stability. Due to its intrinsic instability, the glenohumeral joint has the biggest potential for dislocation compared to other joints of the body [1] and can develop various pathologies. Reported incidence of traumatic anterior instability ranges between 11 and 24 cases per 100 000 people [2], with significantly higher rates in the young and active population. Patients between the ages of 15 and 20 years have show recurrence rates of shoulder instability up to 87% [3].

Over 90% of shoulder dislocations occur in the anterior direction [4] and are associated with injuries to the capsulolabral complex and osseous defects. The treatment of anterior shoulder instability remains controversial and, although conservative treatment is still widely used, surgical repair has been successively more recommended for young patients, since it offers lower recurrence rates, better shoulder mobility and quicker return to activity time [5].

Avulsion of the anteroinferior labrum from the glenoid is the most common injury following traumatic shoulder dislocation [4], so the surgical stabilization procedure generally involves the repair of the detached labrum to the glenoid rim using suture anchors [6]. When large glenoid bone defects are present, however, soft tissue stabilization is not sufficient to restore joint stability [7, 8]. If this situation occurs, a bone grafting procedure for glenoid reconstruction is required. The most common bone grafting technique is the Latarjet procedure, in which the coracoid process is resected and transfered along with the conjoint tendon to the anteroinferior glenoid rim [9].

The original technique has suffered many alterations over the years, like the intra-articular placement of the graft, the improvement of fixation methods and the positioning and orientation of the graft on the glenoid margin. The Latarjet procedure shows very low recurrence rates compared to only capsulolabrar repair techniques [10], however, it is associated with higher complication rates due to the challenging nature of the surgical procedure.

A big long term concern for patients treated with the Latarjet procedure is the development of post-operative osteoarthritis. This complication has shown reported incidence values of up to 58% [11, 12]. Besides the factors of age and number of preoperative dislocations, appearance of osteoarthritis is frequently associated with incorrect positioning of the graft, specifically in a lateral position causing its overhang from the glenoid. However, placing the bone graft medially to the glenoid surface results in higher recurrent rates of instability [13], making some authors believe that the effect of bone augmentation only contributes to joint stability when it reconstructs the glenoid arc and depth [14]. Given these observations, the recommended placement of the bone graft during the Latarjet procedure is flush to the glenoid rim, that is, with its lateral surface adjacent to the articular surface of the glenoid, preferably following its curvature.

Placing the bone graft to exactly follow the articular arc of the glenoid can be very challenging. Clinical studies that have measured the variability of graft positioning during the Latarjet procedure accept different intervals in the medial-lateral direction in which the graft is considered properly positioned (”flush” to glenoid surface) [15, 16, 17]. While some authors believe that the graft can be up to 5 mm medial to the glenoid, others believe that such a high leeway will not guarantee the reconstruction of the glenoid arc and therefore have a diminished effect in restoration of joint stability. Research on optimal graft positioning has been extensive, yet, to the author's knowledge, no study has combined the influence of varying graft medial-lateral placement on both joint stability and glenohumeral articular contact pressure.

Considering that contradicting opinions about the tolerance accepted for the position of the bone graft relative to the glenoid surface exist, the objective of this work was to investigate the best position for bone graft placement during the Latarjet procedure, regarding shoulder stability and contact mechanics, using three-dimensional finite element (FE) models.

1.2 Thesis Outline

This document is subdivided into six chapters, including this first chapter, which contains an introduction to the problem addressed in this work and its main objectives.

Chapter 2 presents a literature review on anterior shoulder instability and the Latarjet procedure, explaining the various concepts used throughout this thesis; introducing the key structures responsible for joint mobility and stability, their failure and respective treatment; and detailing on the Latarjet procedure, by summarizing its current recommendations and complications.

Chapter 3 describes the methodology followed for the development and validation of the FE models of the glenohumeral joint, including the articular cartilages and labrum, and posterior simulation of glenoid bone defects and the Latarjet procedure. Methods for evaluation of the results are also explained.

Chapter 4 displays the results obtained from the FE analyses performed. First, the validation of the healthy glenohumeral joint model is described in terms of stability. Second, the results of the different graft positions are quantitatively assessed.

Chapter 5 discusses the results, through the analysis of the influence of graft positioning on shoulder

stability and articular contact pressure. A comparison with previously published data and the limitations of the current work are also provided in this chapter.

Chapter 6 includes the final conclusions of this study, along with suggestions for future work.

Chapter 2

Background

This chapter presents an overview of anterior shoulder instability and the Latarjet procedure. To do this, it first describes key concepts about shoulder anatomy and stability. The state of the art regarding the recommended position for the bone graft during the Latarjet procedure is also provided.

2.1 Shoulder Functional Anatomy

The human shoulder is a joint complex, composed of four joints and characterized by its large range of motion (ROM). This, however, does not come without its disadvantages as the stability of the joint complex is much more intricate and fragile compared to other joints of the human body. To compensate for its unstable bony geometry, the shoulder relies heavily on muscle and ligaments which act as dynamic and passive stabilizers [18]. In this section, the anatomic and physiological characteristics that contribute to the correct functioning of the shoulder are described, with greater focus on the stabilizing structures related to anterior shoulder instability.

2.1.1 Bones

The three bones of the shoulder complex most significant for its mobility are: the humerus, the scapula and the clavicle. The latter two form the components of the shoulder girdle [19].

The clavicle, presented in Figure 2.1, is an S-shaped bone positioned horizontally above the first rib [19]. It is the only bony connection between the trunk and shoulder girdle by articulating with the sternum medially, which forms the sternoclavicular joint, and with the acromion of the scapula laterally, which forms the acromioclavicular joint. The shaft and lateral end of the clavicle serve as a site for several muscular and ligament attachments [18].

The scapula, also know as shoulder blade, is a flat, triangular bone, as illustrated in Figure 2.2. Its thin and wide configuration provides a large surface for muscle attachments which contribute to its mobility and stabilization [21]. The spine of the scapula, a ridge that crosses its posterior surface, divides the bone into two concave areas: the supraspinous fossae, which serves as an attachment for the

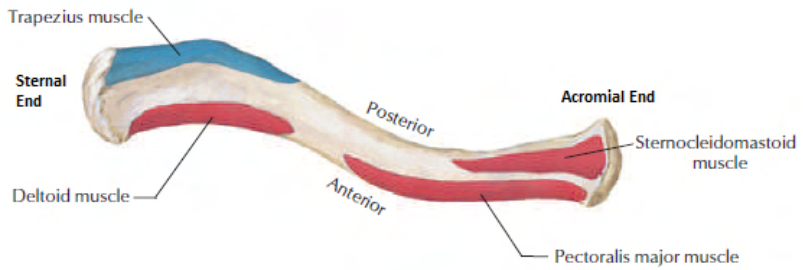

Figure 2.1: Superior surface of the clavicle detailing its muscular attachments. Adapted from [20].

supraspinatus muscle; and the infraspinous fossa, which serves as an attachment for the infraspinatus muscle. The anterior surface of the scapula has a broad concavity called the subscapular fossa, onto which the subscapularis muscle attaches [22]. The lateral end of the spine extends into a flattened and expanded process called acromion, which articulates with the clavicle. Inferior to the acromion and on the lateral apex of the triangle, sits the glenoid cavity, a shallow concave surface that articulates with the humeral head to form the glenohumeral joint. The coracoid process is a thick curved process that projects forward and slightly laterally from the anterior side of the scapula. The coracoid process serves as an attachment for muscles, its tip being the origin of the coracobrachialis muscle and the short head of the biceps brachii, through their junction at the conjoint tendon, as well as the insertion of the pectoralis minor muscle [18].

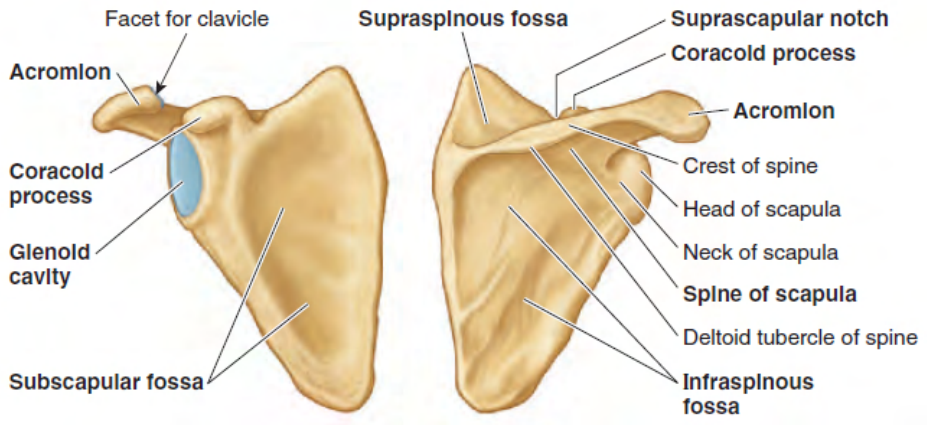

Figure 2.2: Representation of the scapula. Adapted from [22].

The humerus is the longest and largest bone in the upper limb. Its proximal end consists in a head, surgical and anatomical necks, bicipital or interturbecular groove, and greater and lesser tuberosities, as represented in Figure 2.3. The humeral head is a half spheroid which articulates with the glenoid cavity of the scapula [18], forming the glenohumeral joint. Located at the junction between the head and neck and the shaft of the humerus, the greater and lesser tuberosities stand on opposite sites of the bicipital groove and serve as site for insertion of the rotator cuff tendons [18]. The distal end of the humerus articulates with both the radius and ulna at the elbow joint. On its lateral and medial side are two prominent features called the epicondyles, which serve as sites for muscular attachment [19].

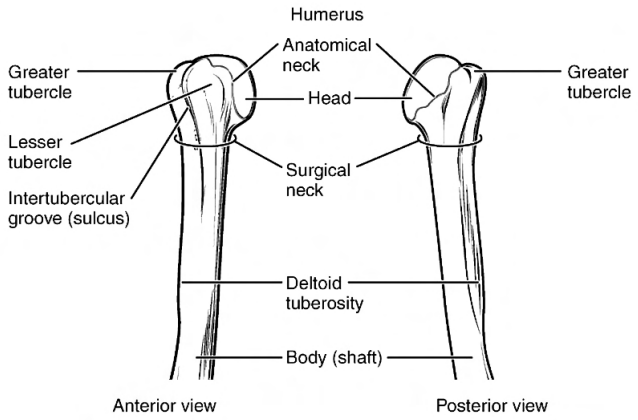

Figure 2.3: Anterior and posterior view of the proximal humerus. Adapted from [23].

2.1.2 Joints

The shoulder complex is characterized by its mobility, which is the highest of all the joints in the human body, with a ROM that covers almost 65% of a sphere. This large mobility stems from of the combined motion of its joints, specifically the sternoclavicular (SC), the acromioclavicular (AC), the scapulothoracic (ST) and the glenohumeral (GH) joints [24].

The SC joint, shown in Figure 2.4, is a small synovial joint located at the base of the neck and consists in the articulation between the clavicle, the manubrium of the sternum and the first costal cartilage. It acts as the only connection between the upper limb and axial skeleton. It is divided into two compartments by a fibrocartaliginous articular disk, which is attached to three ligaments, conveying great strength to this joint [18]. Besides strength, the SC joint also shows significant mobility, allowing clavicular elevation of 11° –15° , retraction of 15° –29° during arm elevation and axial rotation of up to 40° [24].

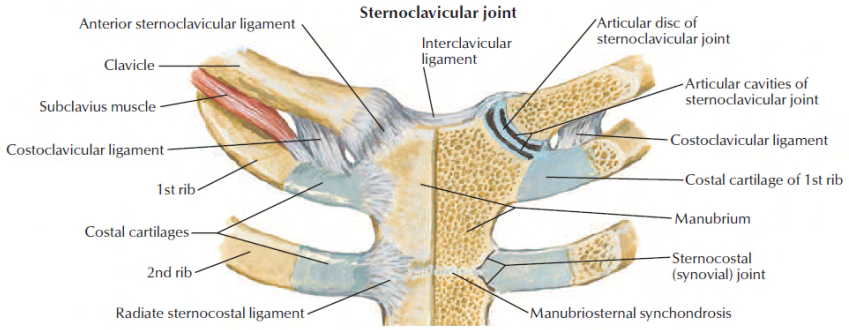

Figure 2.4: Representation of the sternoclavicular joint. Adapted from [20].

The AC joint is a synovial joint resulting from the articulation between the lateral end of the clavicle and a small facet on the acromion of the scapula. Its stability is assured by the superior and inferior acromioclavicular ligaments that reinforce the weak joint capsule [25]. The AC joint allows rotation of the scapula on the acromial end of the clavicle, increasing its range of rotation. This movement is associated with the motions of the physiological scapulothoracic joint [22].

The ST joint refers to the articulation of the scapula with the thorax. Although commonly refered to as a joint, it is not a true anatomic joint. It is occupied by neurovascular, muscular, and bursal structures

that allow the movement of the scapula on the thorax and enhance GH stability [18]. The most important motion of the scapula is the upward rotation, which permits an increase on the range of elevation of the arm, beyond the 120° offered by the GH joint [18].

The GH joint, normally referred to as the shoulder joint, is a ball-in-socket synovial joint which articulates the humeral head and the glenoid fossa of the scapula. This joint possesses the largest ROM of any diarthrodial joint in the body allowing flexion/extension, abduction/adduction, internal/external, rotation and circumduction. This large mobility is due to the mismatching size of the articular surfaces as the humeral head is approximately 3 times larger than the glenoid's surface area [26]. Even though the GH joint shows great physiological motion, the displacement of the humeral head remains quite small in the healthy individual [27, 28]. This stability of the humeral head is accomplished through the interplay of ligamentous structures and surrounding shoulder musculature [29]. Even with the effect of multiple stabilizers, the GH joint remains fragile, being one of the most dislocated joints in the body [1]. The articulation of the humeral head with the scapula is represented in Figure 2.5.

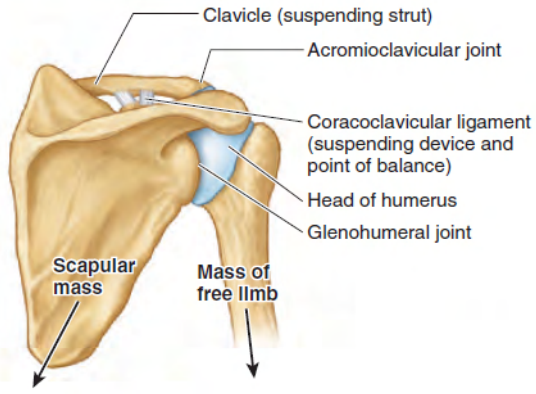

Figure 2.5: Posterior view of the articulation between the humerus and the scapula. Adapted from [22].

2.1.3 Passive Stabilisers

Passive stabilization of the shoulder is assured by the capsulolabral ligamentous complex, producing a concavity compression effect that is magnified by the active muscle forces. Concavity compression refers to the stability gained by the compression of the humeral head into the concave glenoid cavity [30], so the deeper the cavity, the more stable the joint. Concavity compression in the GH joint is possible due to the conformity of the articular surfaces. Although the bony radius of curvature of the scapula is flatter than that of the humeral head, the glenoid cartilage has variable thickness, making both surfaces approximate the shape of a sphere [26]. The capsulolabral ligamentous complex is comprised of the glenoid labrum, GH joint capsule and the ligaments connected to it.

The glenoid labrum is a dense fibrocartilaginous structure attached to the margin of the glenoid cavity as illustrated in Figure 2.6. It is triangular in cross-section and therefore extends the conforming articular surfaces and deepens the glenoid cavity [18]. Howell and Galinat [31] showed that the labrum contributes to 50% of the depth of the glenoid fossa, and thus to joint stability through concavity compression (Figure 2.7). Both cadaveric and computational studies have shown that loss in the integrity of the labrum reduces the effectiveness of compression stabilization up to 20% [30, 32, 33].

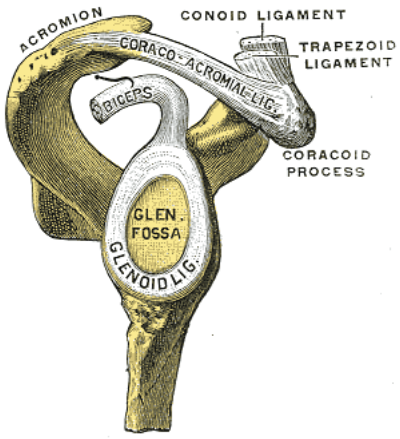

Figure 2.6: Lateral view of the scapula with representation of the glenoid labrum (refered to as glenoid lig.) [34].

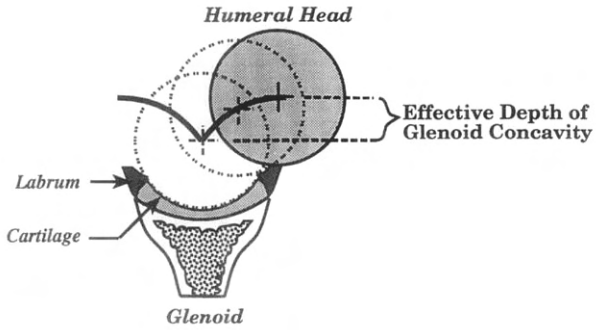

Figure 2.7: Contribution of the labrum to the effective depth of the glenoid concavity [30].

The GH joint capsule is an articular capsule that completely covers the GH joint. Its surface area is approximately twice that of the humeral head, making it a loose structure that allows a large range of motion [18]. During extreme positions of the range of motion, the fibers of the capsule tighten to center the humeral head and limit its displacement. The capsule is reinforced with capsular ligaments which contribute greatly to stability, and, much like the joint capsule, become more important at the limits of motion [29].

The anterior GH capsule connects to three distinct ligaments: the superior GH ligament, the middle GH ligament and the inferior GH ligament [29]. The superior GH ligament functions to restrain inferior translation of the humerus with the arm in neutral position [35]. The middle GH ligament, which is the most variable of the three, resists anterior and posterior translations at mid range of shoulder rotation [35]. The inferior GH ligament is the thickest and most consistent of the GH ligaments [18] and can be divided into three sections:the anterior band, the axillary pouch, and the posterior band. It plays a significant role in restricting anterior and inferior translation at positions beyond 45° abduction and in external rotation [35].

Another ligament important in static stabilization of the shoulder is the coracohumeral ligament. It originates from the coracoid and inserts into the greater and lesser tuberosities, constraining the humeral head's position within the glenoid during arm abduction. Along with the superior GH ligament, the

coracohumeral ligaments also resist posterior translation of humeral head in foward flexion, adduction and internal rotation [18]. Both the GH capsular ligaments and coracohumeral ligament are represented in Figure 2.8.

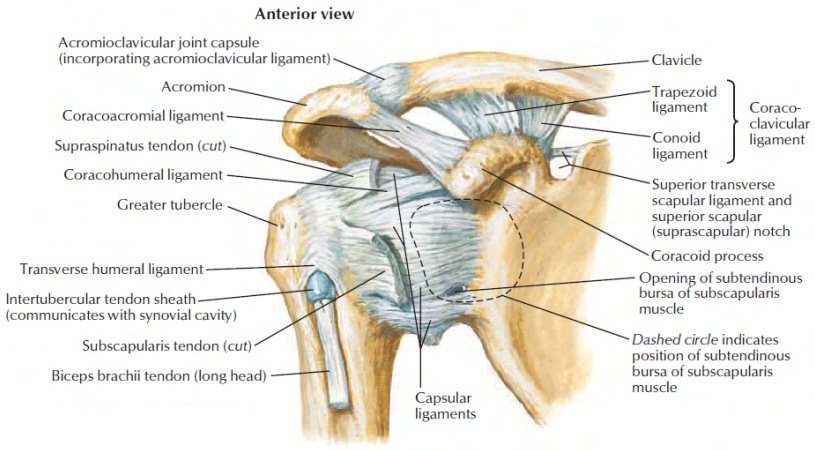

Figure 2.8: Anterior view of the stabilizing ligaments of the GH joint [20].

2.1.4 Dynamic Stabilisers

Dynamic stabilization of upper limb motion is obtained by the cooperative mechanism of various shoulder muscles and mostly focuses on two different points: GH stability and scapulothoracic stability [36]. Figure 2.9 depicts the muscles responsible for stabilizing of the shoulder complex. Most of these muscles play the role of providing support and mobility to the joint.

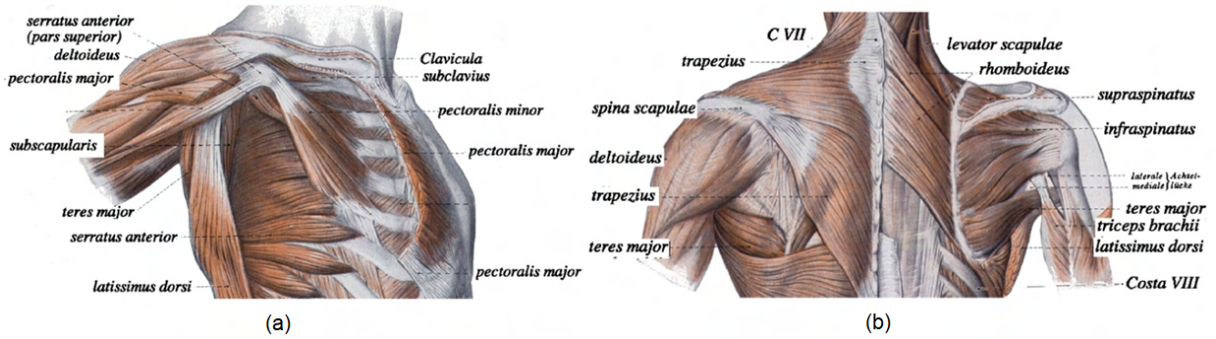

Figure 2.9: Muscles of the shoulder girdle. a) Anterior view of deep muscles, after removal of Pectoralis Major. b) Posterior view of superficial (left) and deep (right) muscles of the shoulder. Adapted from [24].

The primary active stabilizers of the GH joint are the rotator cuff muscles, the deltoid and the long head of the biceps brachii [29]. The rotator cuff is an important group of muscles consisting of the subscapularis, supraspinatus, infraspinatus and teres minor. These are near perpendicular to the glenoid plane, which is defined by the most prominent points of the glenoid rim with its normal pointing outwards from the glenoid concavity. The primary stabilizing effect of the rotator cuff is, therefore, to apply compressive forces that contribute to concavity compression [37]. The direction of the force produced by contraction of each rotator cuff muscle and the resulting net force are represented in Figure 2.10. Besides the compressive effect, the rotator cuff muscles also counteract destabilizing shear forces and

direct the resultant force vector into the glenoid [24]. In terms of motion, the supraspinatus assists the deltoid to allow arm elevation, the infraspinatus and teres minor act as external rotators and the subscapularis functions in internal rotation [18].

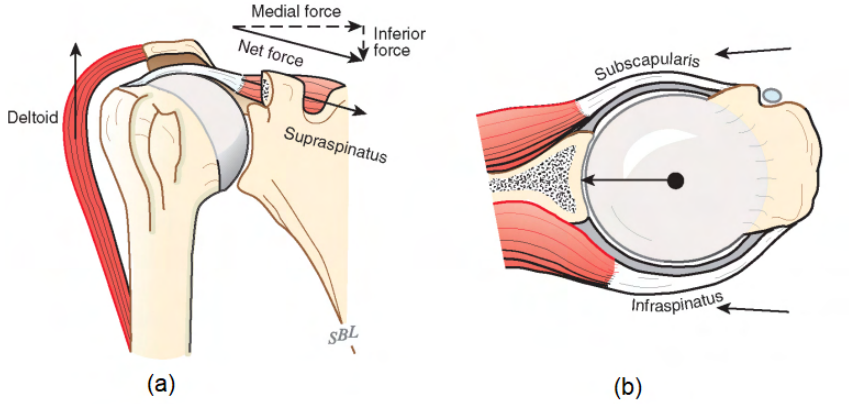

Figure 2.10: The stabilizing action of the rotator cuff. The combined action of rotator cuff produces a force that compresses the humeral head into the glenoid cavity [37].

The long head of the biceps has also been shown to have significant effect in GH stability by reducing anterior translation and resisting external rotation during certain movements [18].

The scapulothoracic musculature serves to stabilize and allow motion of the scapula. These include the trapezius, rhomboids, levator scapulae, serratus anterior, pectoralis minor and deltoid, which are represented in Figure 2.9. Among these, the most important are the trapezius and the serratus anterior. The trapezius is the largest and most superficial muscle, divided into three functional parts: descending (superior), ascending (inferior), and middle. The middle part helps the scapula as a retractor, while the descending and ascending parts function, respectively, as an elevator and depressor [22]. The serratus anterior causes scapular protraction and upward rotation and maintains the medial angle against the chest wall [18]. The levator scapulae works closely with the serratus anterior elevating the superior angle, resulting in upward and medial rotation of the scapula [18].

The rhomboids, consisting of the major and minor muscles, participate in retraction and elevation of the scapula, while the pectoralis minor causes its protraction and inferior rotation. The deltoid, besides contributing to GH stability, is also a scapulothoracic muscle, assisting in forward elevation with the help from the pectoralis major and biceps [18].

2.2 Anterior Shoulder Instability

To better understand the purpose of the Latarjet Procedure, this section first provides an overview of the clinical situation of anterior shoulder instability patients, focusing on injuries and treatments. Then, it focuses on the Latarjet Procedure and state of the art regarding its consequences and recommendations.

2.2.1 Natural History

The bony geometry of the GH joint gives it great flexibility at the expense of stability, making it the most commonly dislocated joint in the human body. The incidence of traumatic shoulder instability in the general population has been reported to range between 11 and 24 cases per 100 000 people [38, 39, 2], with over 90% occurring in the anterior direction [38, 4, 2]. Therefore, the study of the injuries leading to anterior shoulder instability and its treatment is of significant importance to the general population.

Overall, the majority of reported shoulder dislocations happens in the young population [38, 40, 2, 41], these being mostly due to high energy injuries associated with contact sports. Incidence also increases among the elderly population generally associated to fall incidents [40].

The compromise of the stabilizing structures of the joint often leads to recurrent instability, particularly among young patients [1, 42]. Re-dislocation of the shoulder commonly occurs until 2 years after the initial dislocation. The high recurrence of anterior shoulder dislocations can be attributed to the shoulder anatomy deformities present following initial dislocation, like abnormal laxity of the joint capsule and surrounding muscles, deformities of the head of the humerus, and contracture of the muscles surrounding the GH joint [5].

The most common injury following an instability event is the avulsion of the anteroinferior labrum from the glenoid rim [4], known as a Bankart lesion (Figure 2.11). This lesion shows prevalence rates of up to 73% in shoulder instability cases [43, 44], seemingly increasing after recurrence [45]. Avulsion of the anteroinferior labrum can be accompanied by other injuries to the capsulolabral ligamentous complex like capsular tears or humeral avulsion of the GH ligament [46].

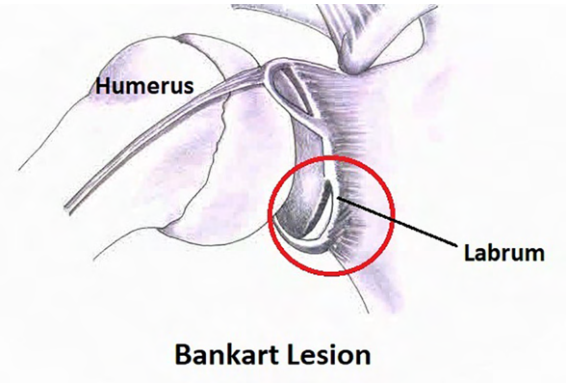

Figure 2.11: Avulsion of anteroinferior glenoid labrum [47].

Due to the shifting of the humeral head, a bankart lesion can also lead to the fracture or erosion of the anterior glenoid rim, named a Bony Bankart lesion. Although it was first believed to happen on the anteroinferior margin of the glenoid, studies have shown that glenoid bone loss happens more frequently on the anterior side [48, 49]. As can be seen in Figure 2.12, erosion of part of the glenoid surface will cause it to become flatter, and therefore less resistant to shear forces, increasing the risk of dislocation [50]. Increasing bone loss in the glenoid has been shown to decrease shoulder stability under compressive loads [8], increase contact pressures and decrease contact area [51].

Another frequent bony injury associated with shoulder instability is the Hill-Sachs lesion. This is

an impression fracture in the postolateral aspect of the humeral head caused by its impact with the glenoid rim as it dislocates anteriorly. When both an osseous glenoid defect and a Hill-Sachs lesion are present, their relative positions can be determining for the choice of treatment. If the Hill-Sachs lesion is oriented so that it engages with the glenoid bone defect under functional abduction or external rotation, the patient will experience symptoms similar to that of subluxation [50] and joint stability can be highly compromised [52].

There are some less common injuries which can occur in the GH joint after dislocation. Some examples are the anterior labral periosteal sleeve avulsion lesion, a Bankart variant where the avulsed periosteum remains intact [4], or the superior labrum anterior to posterior lesion, where the avulsion of the anteroinferior labrum extends to the superior labrum.

In elderly patients, anterior shoulder instability can be accompanied by rotator cuff tears, which predominantly involve the tear of the supraspinatus muscle [53]. The overall frequency of rotator cuff tears increases with advancing age, with reported incidence of over 40% in patients above 40 years old [54]. However, this is not often encountered in young patients and is usually adequately solved through the repair of the torn tendon [63].

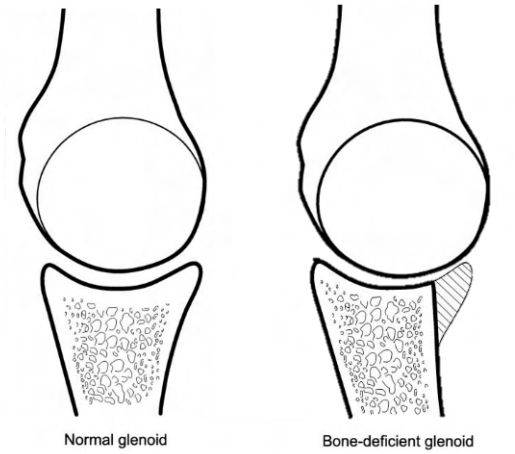

Figure 2.12: Comparison of a normal (left) and a bone-deficient (right) glenoid. The bone deficient glenoid presents a flatter cavity and smaller arc. Adapted from [50].

2.2.2 Treatment

Anterior shoulder instability can be managed through non-operative or surgical treatment. Non-operative treatment mostly consists in immobilization, activity restriction and exercise rehabilitation [55]. The objective of physical therapy is to achieve adequate range of motion, stretch the antagonists of the shoulder joint and strengthen rotator cuff and other muscles that support the scapula [56]. However, different studies have reported high rates of recurrent instability in young, athletic patients following non-operative treatment [57, 58]. This led to surgical treatment being increasingly recommended to younger patients with shoulder instability, especially those who participate in contact sports [59], so the number of patients treated surgically has grown over the years.

Since a Bankart lesion is the most common injury following a shoulder dislocation event, surgical stabilization generally involves the repair of the detached labrum to the glenoid rim using suture anchors

[6], as seen in Figure 2.13. This procedure, denominated as Bankart repair, can significantly reduce recurrence rates when compared to non-operative treatment [60, 58, 57]. Nevertheless, these rates have been reported to be as high as 67% in patients with large glenoid bone loss or Hill-Sachs lesion engaging with the anterior glenoid rim [50]. This indicates that the size of the glenoid bone defect may affect the effectiveness of Bankart repair in restoring joint stability [33].

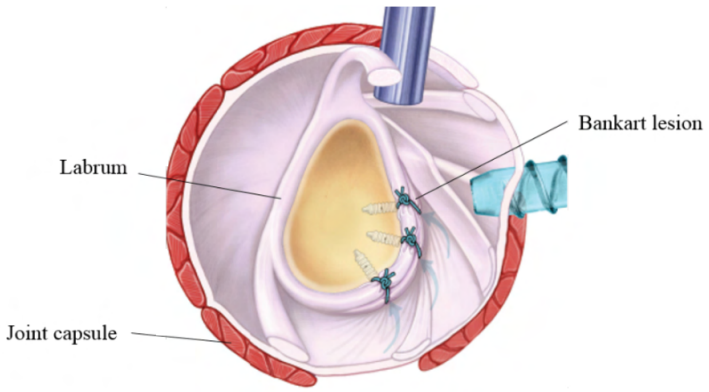

Figure 2.13: Representation of Bankart repair using 3 suture anchors [61].

Cadaveric studies reported an inverse relationship between stability and the amount of glenoid bone loss, demonstrating that a bone defect with a width bigger than 20% of glenoid length significantly decreases the stability of the joint [8, 7]. This value is therefore used by some surgeons as the critical size of a glenoid bone defect after which a bone augmentation procedure is recommended, instead of a soft tissue procedure like labral repair.

There are different bone augmentation or bone grafting procedures to treat shoulder instability; however, the most commonly used is the Latarjet procedure [9]. This techique uses the coracoid process as a bone graft, transferring it to the anteroinferior side of the glenoid along with the conjoint tendon. Since this procedure is the focus of this work, it is thouroughly explained in the next section.

Another reason for recurrence after Bankart repair is the presence of Hill-Sachs lesions that engage with the anterior glenoid rim [50]. An engaging Hill-Sachs lesion is defined as one that presents the long axis of the defect parallel to the anterior glenoid with the shoulder in a functional position of abduction and external rotation. When the patient has this kind of injury, a Remplissage intervention is recommended to better restore shoulder stability [62]. The Remplissage procedure involves the attachment of the infraspinatus tendon to the humeral defect to fill the Hill-Sachs lesion [3] and is illustrated in Figure 2.14. This filling of the humeral defect prevents the Hill-Sachs lesion from engaging on the rim of the glenoid [3]. Depending on the other injuries present, this intervention can be alongside a soft tissue procedure or a Latarjet procedure.

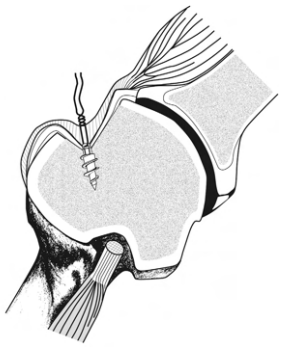

Figure 2.14: Remplissage procedure using the infraspinatus tendon to fill the Hill-Sachs lesion [64].

2.2.3 Latarjet Procedure

The Latarjet technique was first described in 1954 [9] but still remains an effective method for patients with recurrent instability or large glenoid bone defects [65]. Traditionally, the procedure consists in the osteotomy and transfer of the horizontal coracoid process along with the conjoint tendon to the anteroinferior glenoid rim and its fixation with cortical screws (Figure 2.15). The technique has had many suggested alterations over the years, from the intra-articular placement of the graft (as opposed to the original extra-articular placement) to different fixation methods that are still studied today [65]. The traditional procedure was performed with open surgery but its arthroscopic version, first described by Lafosse et al. [66], is becoming increasingly popular.

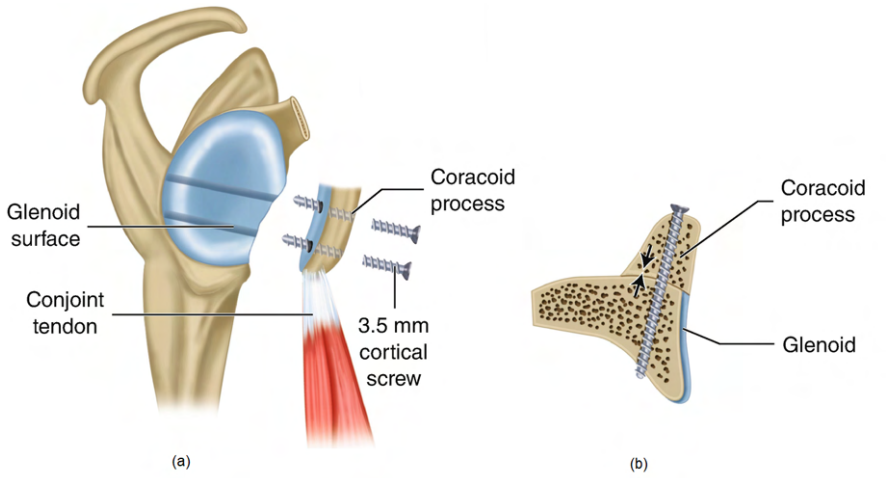

Figure 2.15: Lateral (a) and cross-sectional (b) view of the Latarjet procedure [67].

The efficacy of the Latarjet procedure is explained by three different processes, know as the ”triple locking effect” [68]. First, the coracoid graft serves as a bony extension of the glenoid concavity, increasing the articular arc available for translation before dislocation, known as the ”bone effect”. Second, the conjoint tendon acts as a sling, resisting anterior translation of the humerus during abduction and external rotation, and as a hammock, lowering the subscapularis muscle so that it reinforces the capsule (Figure 2.16). Third, the capsule is repaired and reinforced by reattaching the coracoacromial ligament.

The addition in stability provided by the sling effect is the reason the Latarjet procedure is the most common technique aiming at bone reconstruction of the glenoid. Other techniques use iliac crest bone

graft or tibial plateau allograft, which tend to follow the contour of the glenoid and do not disrupt the original anatomy of the shoulder but lack the effect of the conjoint tendon [3].

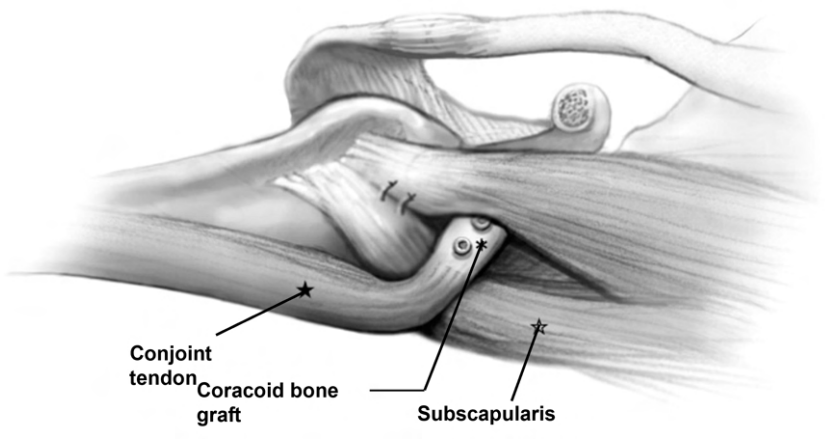

Figure 2.16: Sling effect: In positions of high external rotation, the conjoint tendon works as a ”sling” adding tension to the inferior portion of the subscapularis to resist anterior humeral head translation. Adapted from [14].

In an effort to quantify the significance of each of the proposed effects of the Latarjet procedure for restoration of joint stability, Yamamoto et al [14] performed a cadaveric study measuring the anterior translational force necessary to dislocate the joint after performing the procedure. By testing different conditions of the involving soft tissues, they concluded that the sling effect was the main contributor for joint stability, be it at a mid range position (60° GH abduction and neutral external rotation) or at an end range position (60° GH abduction and maximum external rotation). With the arm at a mid range position, however, the effect of osseous reconstruction of the glenoid still had a significant effect, accounting for 38% to 49% of the restored stability.

Outcomes

This technique shows very good clinical outcomes [69, 13, 70], with recurrence values below 7% [10]. However, several other complications have been reported, associated with the challenging nature of the surgical procedure and the position of the graft. One such complication is bone graft non-union or fibrous non-union. A bleeding surface in the graft and scapula should be created to allow union between these structures; nevertheless, non-union of the graft and scapula can also occur due to single screw fixation [10]. Loss of external rotation and shoulder stiffness is also a significant concern for patients, even though high satisfaction scores are reported post-procedure [12]. Stiffness of the shoulder is highly associated with the technique used for subscapularis tenotomy [71]. Similarly, reported cases of neurovascular injury can be avoided with adequate surgical technique.

A frequent event following this surgery is the partial lysis of the coracoid graft [12], which can cause pain and discomfort if the screw head becomes too proud. Osteolosysis of the graft can be associated to both biomechanical and biological factors. From a biomechanical point of view, the change in mechanical loading of the resected coracoid leads, according to Wolff’s law, to adaptation of the bone remodelling

process. To this end, the fixation method used in the Latarjet Procedure has been investigated to improve graft osteolysis results. Sano et al. [72] showed, in a computational study, that the stress shielding effect was most evident in the proximal part of the graft. This was in accordance with several reports claiming that osteolysis is most proeminent in the proximal part of the graft [69, 73, 74]. A recent computational study [75] compared the traditional cortical screw fixation to two new introduced methods (wedge profile plate and endobutton) to improve graft fixation and osteolysis, concluding that the endobutton generates lower compressive forces.

A concerning long term outcome of the Latarjet procedure is the development of postoperative osteoarthritis [11]. Follow-up studies of patients undergoing this procedure report a presence of arthritis in up to 58% of shoulders [12, 11]. The majority of cases demonstrate only mild arthritis, with risk factors being older age, high-demand sports and lateral overhang of the graft [11]. The positioning of the graft during the Latarjet procedure is highly discussed and its review is presented in the next section.

Graft Positioning

The position of the graft is considered essential for the outcome of the Latarjet procedure. Records show that, if placed too laterally, the overhanging of the graft may damage the cartilage of the humeral head and promote early osteoarthritis [12, 13]. However, if placed too medially, it results in higher recurrent instability compared to a more lateral position [13].

Osteoarthritic changes in the humeral head cartilage can be attributed to a shift in joint alignment and incongruity of the articular surfaces. The overly lateral placement of the graft causes it to become proud of the glenoid surface, decreasing its congruity with the humeral head. It will also cause a shift in the seating of the humeral head in the glenoid, not allowing proper alignment of the joint. Ghodadra et al. [76] used a biomechanical study to evaluate differences of articular contact pressures in different positions and orientations of the graft. They showed that a lateral position increases peak articular contact pressure in the anteroinferior quadrant of the glenoid and shifts the contact pressure posteriorly, which plays an important part in the increased risk of osteoarthritis.

A graft placed too medially to the glenoid surface also has its consequences. The first described mechanism of the ”bone effect” of the Latarjet surgical technique was the use of the bone graft as extension of the glenoid that served merely as medial block to the humerus [68]. However, some authors believe that joint stability is restored through a glenoidplasty effect [14], which consists in the reconstruction of the glenoid arc. This effect can only be achieved if the bone graft is positioned exactly flush to the glenoid margin so its curvature continues the arc, as illustrated in Figure 2.17. Nevertheless, the exact influence of the graft positioning in shoulder stability is not properly quantified in the current literature.

Positioning the graft exactly aligned to the glenoid articular surface can be challenging, especially during the arthroscopic procedure, so when evaluating it a certain tolerance has been accepted. Different methods are used to quantify this position: using the perpendicular distance to a virtual straight line defined from the posterior edge to the anterior edge of the glenoid in the axial plane [17, 16]; or the distance between the tip of the bone block and a circle aligned with the radius curve of the horizontal glenoid bone surface [17]. These two methods are represented in Figures 2.18 and 2.19, respectively.

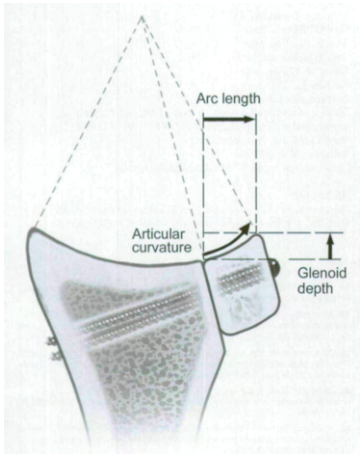

Figure 2.17: Glenoidplasty effect: when positioned flush to the glenoid rim, the coracoid graft reconstructs the articular arc and restores glenoid depth [77].

Some authors consider 1mm to each side of the straight line to be too medial or too lateral [15] while others consider the graft to be ”flush” to the glenoid until 5mm medial to the same line [17, 16]. However, it can be argued that a graft placed 5 mm medial to the glenoid surface does not reconstruct the glenoid arc and therefore does not contribute to joint stability [76]. Considering this, the large range accepted by some authors conveys the difficulty of the surgical technique, specifically regarding proper placement of the graft. The measuring methods described have a high dependence on the orientation of the vertical axis of the scapula [16], which means there may be even greater variability in the reported measurements of graft placement. As studies have concluded, small changes in the graft position can greatly influence the efficacy of the Latarjet procedure. Investigating the impact of bone graft positioning on possible mechanisms causing the failure of this surgical procedure is, therefore, of great significance to the field.

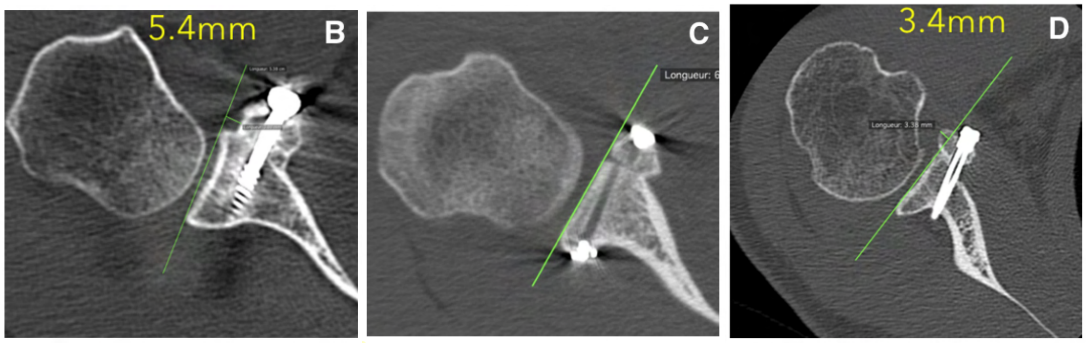

(a) (b) (c)

Figure 2.18: Axial Line Evaluation: Bone graft position in the axial plane (at 25 % or 50 % of the glenoid height) is measured at its most lateral aspect relative to a straight line in the glenoid plane. (a) Graft positioned too medially. (b) Graft in a flush position. (c) Graft position too laterally [78].

The orientation of the bone block recently became a controversial topic as well. The original technique positioned the coracoid so that its lateral edge became juxtaposed to the glenoid surface but this was modified by affixing the coracoid to the glenoid in a rotated position so that the inferior coracoid

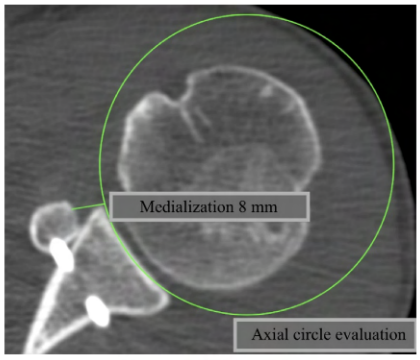

Figure 2.19: Axial Circle Evaluation: Bone graft position in the axial plane is measured at its most lateral aspect relative to a circle fitted to the glenoid arc. The graft depicted presents a medial position [17].

surface became adjacent with the glenoid surface [79]. Authors believed that the inferior surface of the coracoid was more congruent to the articular surface of the glenoid and therefore better able to reconstruct the arc of the glenoid fossa. This technique has shown to optimize contact pressures when compared to the original Latarjet [76] and is able to reconstruct larger glenoid deffects, however, the graft has a lower failure load and is associated to increased graft non-union [80].

2.2.4 Novel Aspects of the Work

Although the effect of bone augmentation in recovering shoulder stability has been discussed in the literature, the relationship between graft position and joint stability is still poorly recorded. This work assesses if the glenoidplasty effect is necessary to restore stability or if only glenoid bone augmentation (the bone graft serving only as block to medial translation) is already sufficient for the purpose. In addition to this, the distribution of contact pressure in the humeral head cartilage is also analyzed, which can provide insight into the mechanisms of the development of osteoarthritis post-Latarjet procedure. Although one study has observed the effect of graft position on contact pressures in the GH joint articular surface, it focused only on the contact pressures of the glenoid, not accounting for the possible contact between the humeral head cartilage and bone graft surface.

Published data studying the Latarjet procedure has been increasing due to the growing use of surgical intervention for treatment of anterior shoulder instability. However, very few computational models of this surgical technique have been developed, none of which possess validation processes. The creation of a FE model of the Latarjet procedure based on a validated shoulder model will allow its use for future studies, contributing to the better understanding of the surgical tecnhique and prevention of its failure.

Chapter 3

Methods

The computational work developed required the creation of FE models with different shoulder conditions. These comprise a model of a healthy GH joint and one with a glenoid bone defect, simulating, respectively, stable and unstable shoulder models. Using the unstable shoulder model as basis, the remaining developed models were of a simulated Latarjet procedure with 4 different graft positions.

The healthy and bone defect models served as basis for the geometry of the Latarjet procedure, so these were validated against cadaveric published data measuring joint stability. Since active stabilizers of the GH joint were not considered in the developed models, the validation processes only refer to passive stabilization.

This chapter gives a detailed description of the geometric and FE modeling steps described above, including the methods applied to validate and evaluate the results.

3.1 Geometric Models

The shoulder model used was based on the one developed by Quental et al. [81, 82]. Only the GH joint geometry was studied in the current work, so the model comprised of the scapula and humerus geometries. To save computational effort, the humerus was cut at its surgical neck and the distal part was excluded from the model, resulting in the geometry present in Figure 3.1. To the previously developed models, the glenoid labrum and articular cartilages were added as these have been proven to contribute to joint stability.

3.1.1 Soft Tissues Geometry

The 3D model geometry of the glenoid labrum was constructed through manual segmentation using the same dataset used in the previously developed models of the humerus and scapula. This process consists in manually delineating the desired structure in each image.

After the manual segmentation process, the 3D model of the labrum was saved as a stereolithography (STL) file and imported into SolidWorks (Education Edition, Academic Year 2020-2021) using the

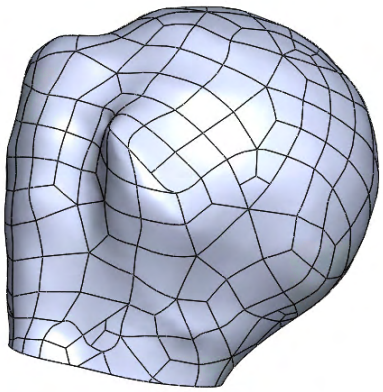

Figure 3.1: Anterior view of the geometric model of the humerus.

ScanTo3D tool. This tool allows the generation of a solid 3D model, application of a smoothing filter to correct staircase effects and imprecise geometry and reduction of the surface mesh.

As the labrum overlapped with the scapula, it was cut using the border of the scapula to make sure the two models aligned perfectly without significant gaps between them. The final model of the labrum, presented in Figure 3.2, was qualitatively validated by the orthopedic surgeon supervisor of this work.

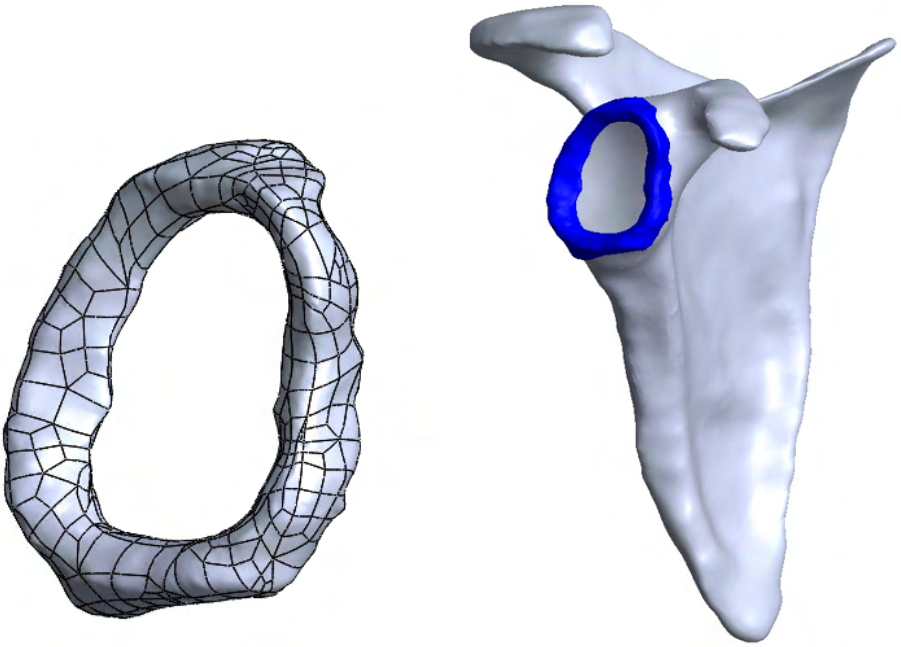

(a) (b)

Figure 3.2: (a) Geomtetric model of the glenoid labrum. (b) Lateral view of the position of the labrum (blue) in the model of the scapula (grey).

The humeral head and glenoid cartilages were also modeled to provide more detail to the GH joint model. Articular cartilage is a thin layer of connective tissue, with thickness ranging from 2 to 4 mm [83]. Because the resolution of the anatomical images used for the development of the geometric models was

not sufficient to accurately portray such thin structures, cartilage tissue geometry was modeled artificially using the SolidWorks software, as performed in previous computational studies [72, 84].

Both the humeral and glenoid cartilage were modeled with a uniform thickness. Although these structures have variable thickness [26, 85, 86], cartilages were simplified assuming thicknesses of 1 mm [85] and 2 mm [26, 86] for the humeral and glenoid cartilages, respectively. To create the humeral cartilage, a portion of the surface of the humeral head was offseted by 1 mm and the space between the this surface and the humeral head was filled to create a solid. The glenoid cartilage was modeled by extruding the surface of the glenoid in a lateral direction, that is, outwards from the glenoid concavity. This cartilage was sliced through the border of the labrum, aligning the side of the cartilage to the labrum, since these anatomical structures are connected.

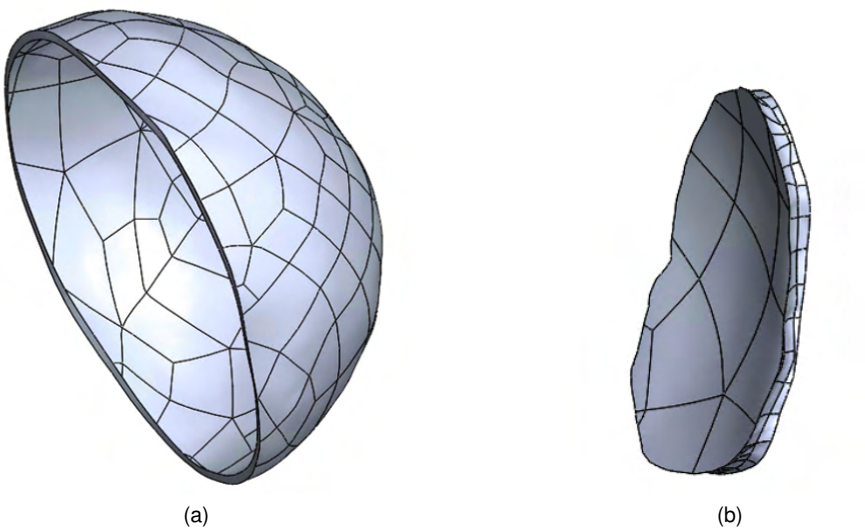

(a) (b)

Figure 3.3: Anterior view of the geometric models of the humeral head cartilage (a) and glenoid cartilage (b).

3.1.2 Creation of Glenoid Bone Defects

The Latarjet procedure is used to treat anterior shoulder instability, especially when the glenoid presents large bone glenoid defects. To this end, different shoulder models with 4 glenoid defect sizes were develop to investigate anterior instability and to validate the shoulder model to which the Latarjet procedure was applied.

Glenoid bone defects have been show to be nearly parallel to the long axis of the glenoid in the anterior direction [48, 49]. To simulate these, the process described by Yamamoto et al. [8] was followed. On the glenoid plane, the long axis of the glenoid was drawn by uniting the superior and inferior contact points of the circumcircle that fit the superoinferior diameter of the glenoid. Osteotomy lines, shown in Figure 3.4, were defined parallel to this axis. The reference line was considered tangential to the anterior rim and the remaining lines were set at varying distances from the reference, measured on the axis perpendicular to the long axis of the glenoid. These distances corresponded to 8%, 14%, 20% and 26% of the glenoid length (Figure 3.4). To create the defects, the glenoid portion of the scapula was

sliced using a plane that passed through the desired osteotomy line and was normal to the surface of the glenoid.

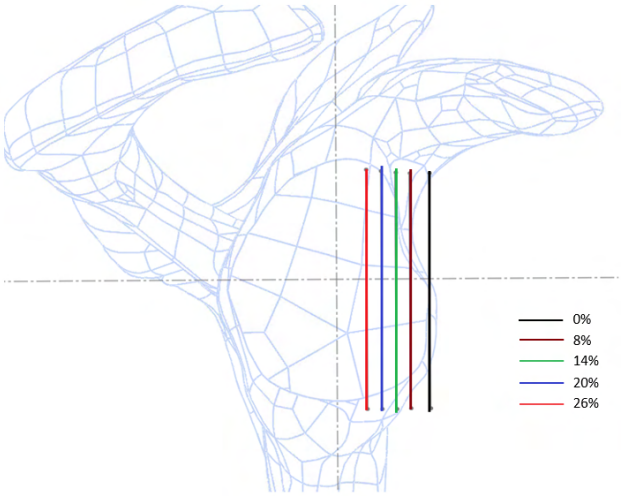

Figure 3.4: Osteotomy Lines were drawn parallel to the vertical axis of the glenoid representing 8%, 14%, 20% and 26% of the glenoid height.

In cases of anterior shoulder instability with a bony Bankart lesion, the labrum can be reattached to the glenoid rim via Bankart procedure. However, in many cases with large bone defects, the anterior portion of labrum degenerates due to its lack of support. For simplicity, the latter case was modeled in this work and the labrum was sliced along with the scapula during the creation of bone defects, as implemented in some cadaveric studies [14, 87].

For simulating the Latarjet procedure, the model of the scapula with a 20% bone defect (Figure 3.5) was selected, being the limit for which the Latarjet procedure is recommended by some surgeons.

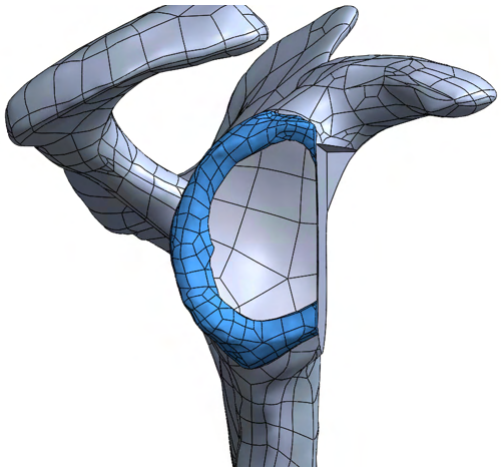

Figure 3.5: Geometry of the scapula (gray) and glenoid labrum (blue) with a simulated 20% bone defect.

3.1.3 Latarjet Procedure

The distal part of the coracoid was resected, making sure the resected part had a length between 22 mm and 27 mm [65]. This cut is represented in Figure 3.6. The cut scapula and coracoid parts were exported as STL files and imported back into the bone defect model.

Figure 3.6: Resection of the Coracoid Graft at its elbow.

Positioning of the coracoid graft was done under the guidance of an orthopedic surgeon (Dra. Clara de Campos Azevedo). The graft was rotated and positioned so that its lateral edge followed the curvature of the glenoid surface. Attention was also given so that it did not become proud relative to the articular surface when observed from an anterior perspective. The inferior side of the coracoid process was sliced using the scapula as basis, which created a flat decorticated surface congruent with the defect model of the scapula. Figure 3.8 shows the model of the scapula and corresponding soft tissues after modeling of the Latarjet procedure.

To fix the graft to the scapula, two 3.5 mm cortex screws, depicted in Figure 3.7, were modeled in Solidworks based on the DePuy Synthes' specifications (Universal Small Fragment System). The cortex screws were fully threaded with base and crest diameters of 2.4 mm and 3.5 mm, respectively. The length of these components was chosen as 30 mm considering the size of the glenoid neck. The placement of the screws is illustrated in Figure 3.8b. These were placed in a centered position of the graft's exterior surface, with a minimum distance of 7.5 mm between their respective centers and inserted in a direction parallel to the glenoid surface plane.

Four configurations were considered for the graft position by varying its position medio-laterally. Considering the position indicated by the surgeon as the reference, the graft was translated 1.5 mm, 3 mm and 4.5 mm in the lateral direction. No translations were considered in the medial direction because they were assumed to behave similarly to the reference position as far as shoulder stability is concerned.

To categorize these positions with respect to the glenoid surface, the methods described in section 2.2.3 were used. The axial line method consisted in measuring the distance of the most lateral aspect of

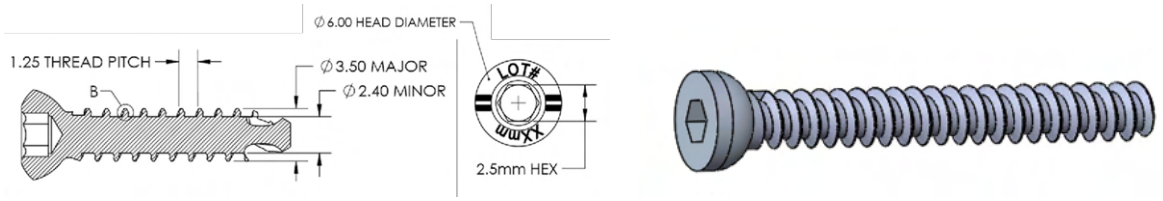

(a) (b)

Figure 3.7: (a) Specifications of a 3.5 mm cortex screws. (b) Modeled geometry of the cortex screws.

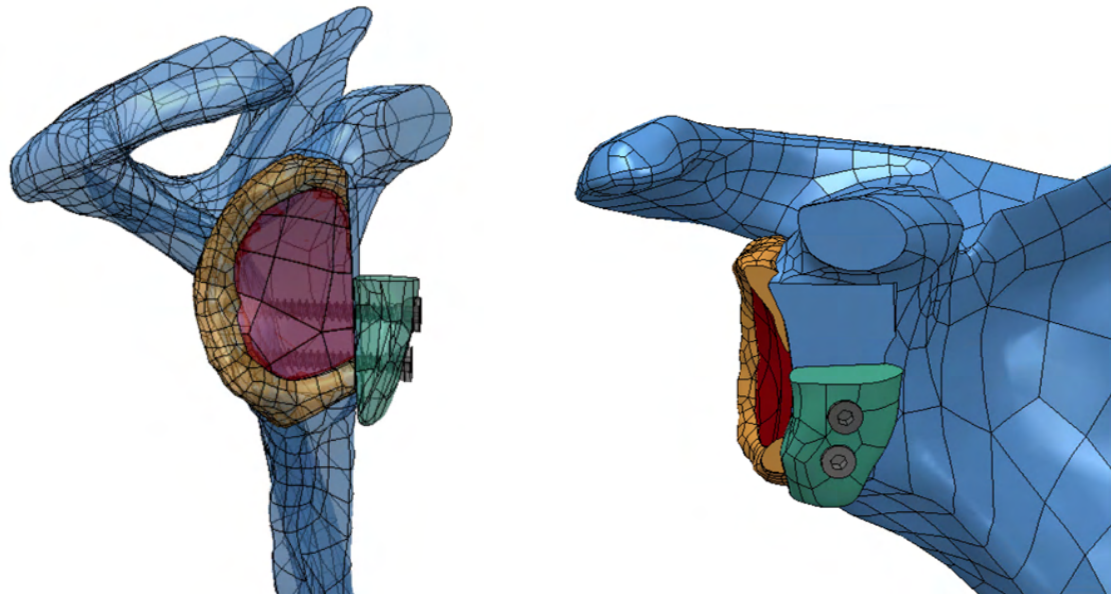

(a) (b)

Figure 3.8: Lateral (a) and anterior (b) view of the glenoid model after the Latarjet procedure with bone graft in the reference position.

the graft relative to the joint line. This joint line is drawn in an axial plane at the level of the upper screw, by connecting the two most lateral points of the glenoid rim. Since the glenoid cartilage was modeled, the joint line was constructed passing through the edges of the cartilage instead of the glenoid. The distance was therefore calculated relative to the articular surface [17]. The axial circle method made use of the same axial plane, but the distance was measured relative to a circle fitted to the glenoid articular arc.

To define the axial plane, the scapula plane was first constructed according to Bryce et al. [88]. They define the scapula plane as the plane passing through three features of the scapula: the most distal point of the inferior scapular angle, the center of the glenoid fossa, and the point at the vertebral border where the scapular spine intersects the medial border of the scapula. The axial plane is the plane perpendicular to the scapula plane at the level of the transverse line, which is the line connecting the two latter points. The different positions of the coracoid graft evaluated using the two methods are described in Table 3.1 and shown in Figure 3.9.

Table 3.1: Evaluation of graft position using the axial line and circle methods. Distances medial and lateral to the line or circle are considered negative and positive, respectively.

Method	Reference model	1.5 mm model	3 mm model	4.5 mm model
Axial Line (mm)	-1.09	+0.4	+1.89	+3.39
Axial Circle (mm)	-3.20	-1.81	+0.44	+1.23

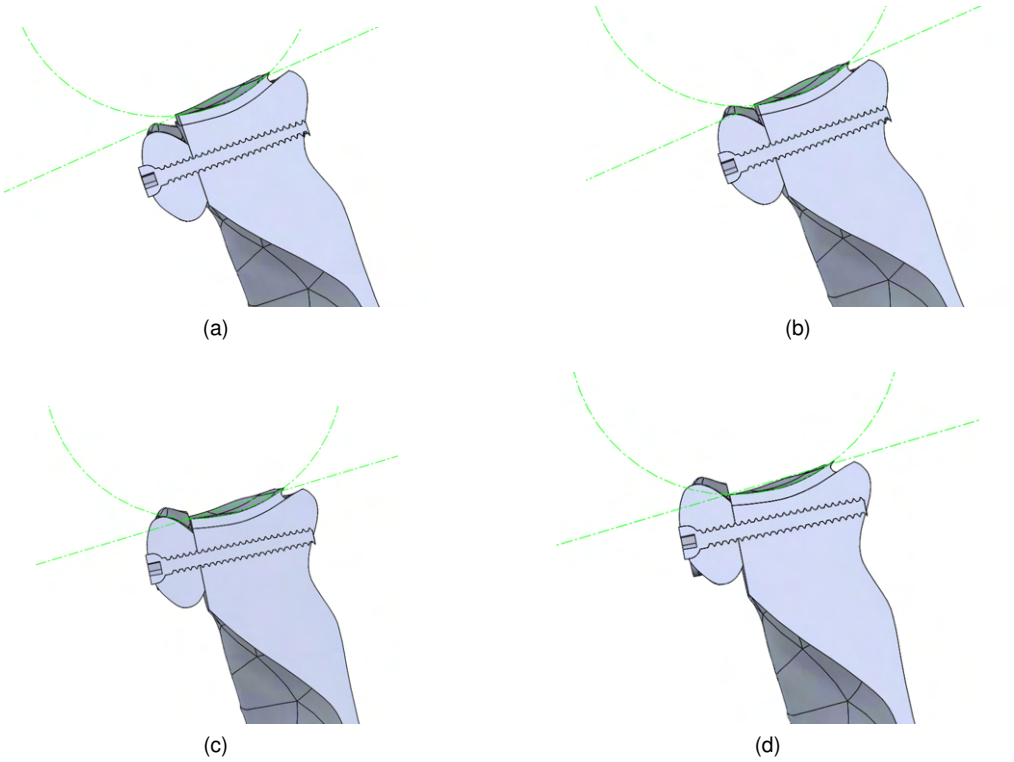

Figure 3.9: Superior view of an axial cross section and evaluation methods of the different modeled graft positions: (a) reference; (b) 1.5 mm; (c) 3 mm; (d) 4.5 mm

3.1.4 Arm Positions

In addition to considering different graft positions, the position of the arm was also varied to evaluate how the Latarjet procedure performed with shoulder motion. The studied positions of the humerus were: neutral position; 30° abduction; 60° abduction; 60° abduction with 45° external rotation. These positions were chosen to replicate common positions studied in the literature [14, 72, 76], allowing better comparison of results. Humeral rotations were modeled according to the humerus and scapula coordinate systems defined by Wu et al. [89]. The axial rotation axis of the humerus, responsible for internal and external rotation, passes through the center of the GH joint and the middle point between the lateral and medial epicondyles. Abduction or elevation of the humerus is the rotation around the GH joint center in the plane formed by the axial rotation axis and the line connecting most posterior point of the acromion and the point at the vertebral border where the scapular spine intersects the medial border of the scapula. As described, these positions were modeled relative to the scapula and not the thorax, so the abduction mentioned refers to GH abduction. Figure 3.10 presents the complete geometric models

of the GH joint after a Latarjet procedure with the various arm positions studied.

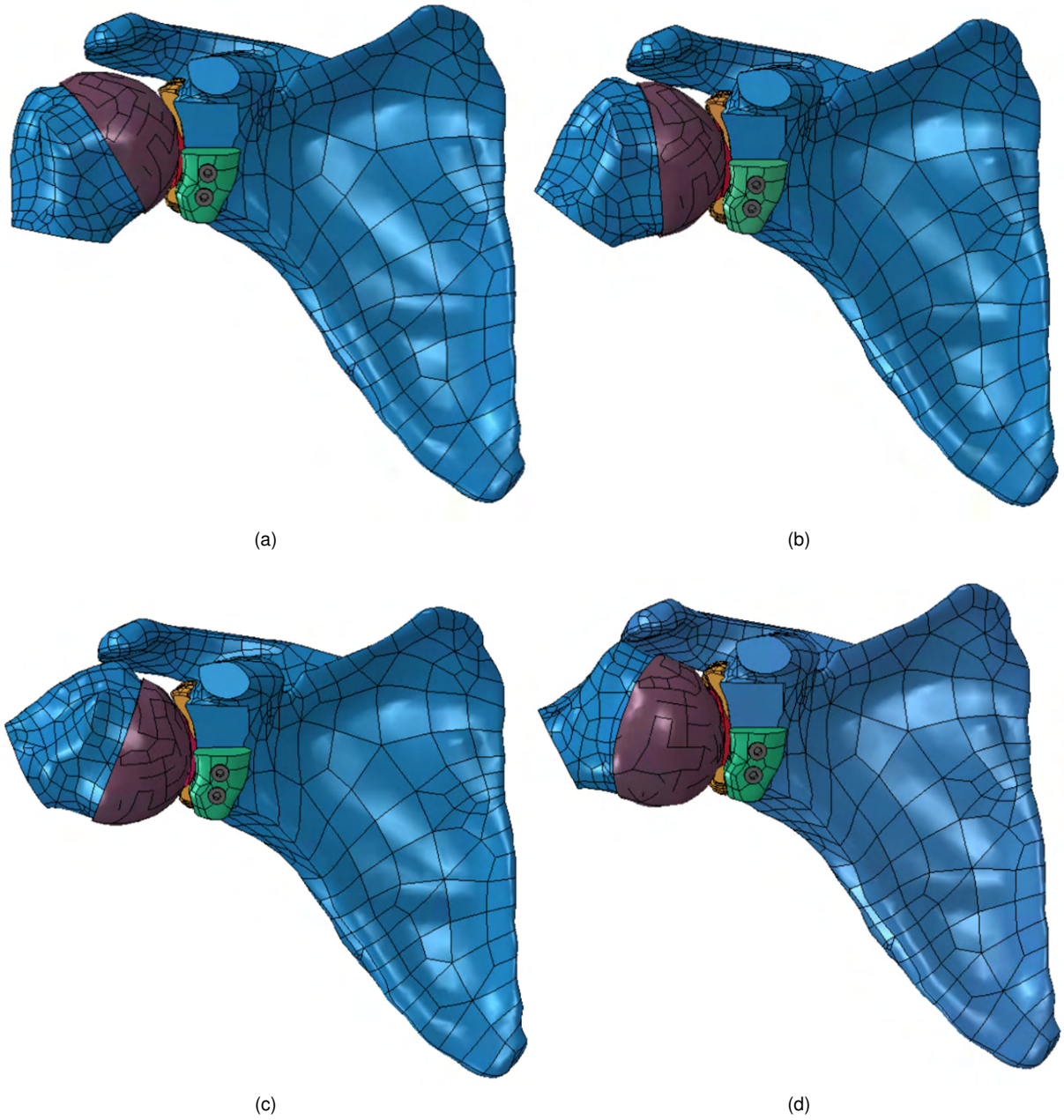

Figure 3.10: Anterior view of Latarjet reference models with different arm positions. (a) Neutral position; (b) 30° glenohumeral abduction; (c) 60° glenohumeral abduction; (d) 60° glenohumeral abduction with 45° external rotation.

3.2 Finite Element Models

Finite Element models of the different configurations described in Section 3.1 were developed using the Abaqus FEA software (version 2017). Each part was imported into Abaqus using STEP format, which placed them automatically in its proper position.

3.2.1 Material Properties

Different materials were assigned to the humerus, scapula, cartilage, labrum and screws. For simplicity in load application, the humerus was defined as a rigid material, which can be justified by the relatively small deformations of bone compared to other soft tissues [90]. However, the coracoid process was in direct contact with the humeral cartilage in the Latarjet models, making its appropriate material definition of higher importance.

The scapula and bone graft were modeled as linear elastic and isotropic materials, for which the Young's modulus depended on bone apparent density. The relationship chosen to represent the material properties of these components was retrieved from *Gupta and Dan* [91], as it is the only numerical model derived directly from the scapular bone [92, 93]. It is given by:

$$\begin{aligned} E &= 1049.45 \cdot \rho^2 \quad \text{for } \rho \leq 0.35 \text{ g/cm}^3 \\ E &= 3000 \cdot \rho^3 \quad \text{for } 0.35 < \rho \leq 1.8 \text{ g/cm}^3 \end{aligned} \tag{3.1}$$

where E is Young's modulus (in MPa) and ρ is bone apparenty density.

The density distribution of the scapula was obtained using an in-house algorithm developed by Quental et al. [94]. Through this algorithm, the density distribution of the scapula was estimated from the computed tomography (CT) images used to create its 3D geometry, by relating the pixel intensity with the bone apparent density [91]. The CT gray values, that is, the average of all attenuation coefficients in each pixel, were converted to Hounsfield units, relating them with the attenuation coefficient of the water. Afterwards, a linear regression was derived using two reference points, representing minimum and maximum bone density.

The modelling of the Latarjet surgical technique caused changes to the scapula's orginal geometry and mesh by dividing it into two parts: the modified scapula and coracoid bone graft. Each of these parts also contained other modifications created by the glenoid bone defect and decortication of the graft. To define the bone densities of the modified scapula and coracoid bone graft, a mapping function was applied to transfer the data from the original geometry of the scapula. The density of each node of the modified scapula was assigned the average density of the most proximal nodes in the original scapula if no node existed in the same coordinates. The density distribution of the coracoid graft was obtained in a similar fashion but a rigid transformation had to be applied to place the coracoid bone graft in its original position before the Latarjet procedure. To identify the rigid transformation to be applied, the same 3 points were identified in the original and modified positions of the coracoid.

Due to the partial volume effect, the apparent density of superficial nodes may be underestimated. To diminish the impact of the partial volume effect, the algorithm was modified so that the nodes corresponding to the external boundary of the original scapula had the maximum density, i.e., 1.8 g cm^{-3}. The density distribution of the scapula and bone graft are represented in Figure 3.11.

Material properties of the different soft tissues and cortex screws are summarized in Table 3.2. The cortex screws are composed of a Titanium alloy. The glenoid labrum and articular cartilages were assigned a hyperelastic, Neo-Hookean material, with strain energy density given by the constitutive law:

$$W = C_{10}(I_1 - 3)$$
$$C_{10} = E/4(1+\nu) \tag{3.2}$$

where E represents the Young's modulus, ν is the Poisson's ratio, and I_1 is the first invariant of the Cauchy–Green tensor.

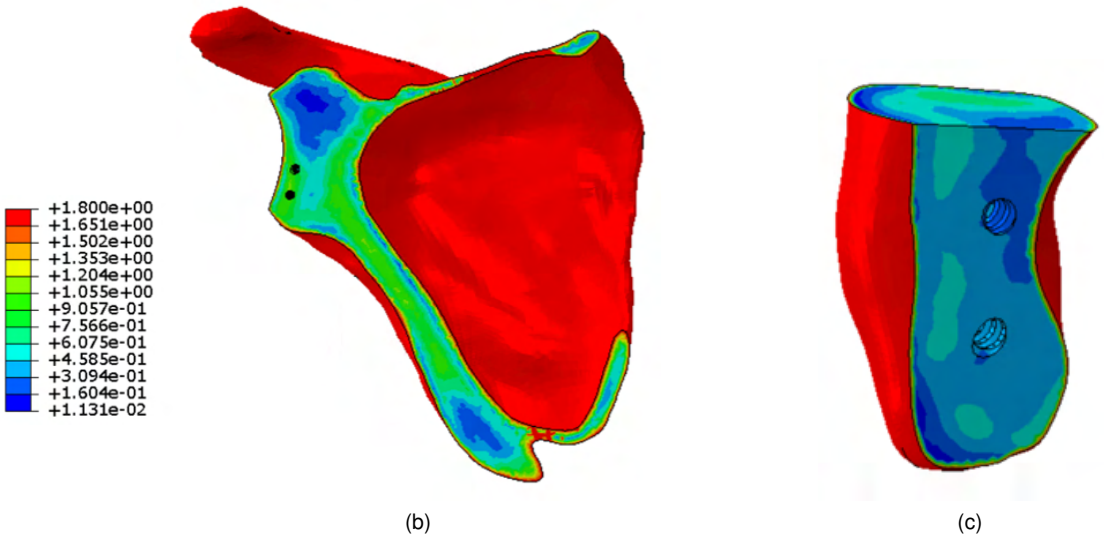

Figure 3.11: Density distribution of the modified scapula and coracoid bone graft. (a) Anterior view of a coronal cut of the modified scapula. (b) View of the bone graft decorticated (inferior) surface

Table 3.2: Material properties of homogenous structures of the finite element models.

Model Part	Material Type	Constants	References
Humerus	Rigid	-	[90]
Cortex Screws	Linear Elastic, Isotropic	$E = 113.8$ GPa , $\nu = 0.3$	[72]
Labrum	Neo-Hokean hyperelastic, incompressible	$C_{10} = 8.3$ ($E = 46.6$ MPa, $\nu = 0.4$)	[95, 96]
Cartilage	Neo-Hokean hyperelastic, incompressible	$C_{10} = 1.79$ ($E = 10$ MPa, $\nu = 0.4$)	[96]

3.2.2 Interactions

The interfaces between the cartilages and their respective bone surfaces, much like the interface between the labrum and glenoid surface or the interface between the labrum and glenoid cartilage, were modeled using a tie constraint. The interactions between the humeral head cartilage and labrum were modeled as frictionless, surface-to-surface contact due the very low coefficient of friction in synovial joints [61, 84]. The interaction of the humeral cartilage with the bone graft was also modeled as frictionless, surface-to-surface contact, as implemented in a previous computational study [72].

A tie constraint was applied to the interface of the modified scapula and decorticated bone graft,

simulating a late postoperative stage, where the union of bone graft and scapula occurred successfully. As the variable studied in this work is the position of the bone graft, the fixation method was simplified by modeling the interaction between cortex screws and interior bone surfaces of the graft and scapula as tied.

To aid the convergence of the simulations, contact stabilization was activated. This stabilization adds virtual viscous forces, which oppose incremental relative motion between surfaces and decrease throughout the simulation, until disappearing at the end. To guarantee the validity of the results, attention was kept so that the maximum dissipated energy was lower than 5% of the maximum internal energy, as recommended in Abaqus documentation.

3.2.3 Boundary conditions

In all FE models, the scapula was fixed using an encastre condition on the nodes shown in Figure 3.12, restricting all displacements and rotations of these nodes [82].

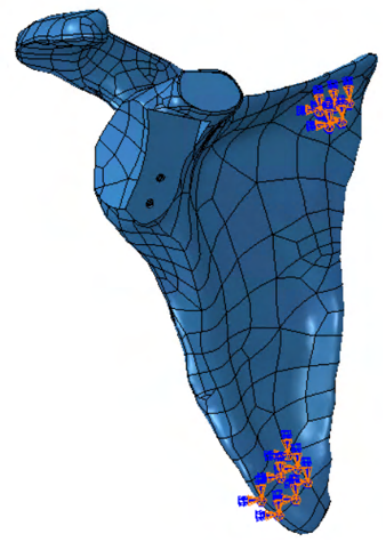

Figure 3.12: Fixation of displacements and rotations of the scapula was made in its anterior side in two different regions.

The loading conditions can be divided into two major steps: (1) compression of the humeral head onto the glenoid; and (2) anterior translation of the humerus. For comparison with the literature, the experimental procedure followed by Lippit et al. [30] was mimicked. The direction of the loads was defined making use of the coordinate system present in Figure 3.13, in which the x and y axis belong to the plane of the glenoid articulating surface and point in the superior and anterior directions, respectively.

The step (1) involved the application of a compressive force through the center of the humeral head in the z direction, that is, perpendicular to the plane of the glenoid articulating surface, turned towards the scapula. This load was applied with a magnitude of 50N. Rotations of the humeral head were constrained to keep the arm position unchanged throughout the simulation. The application of this load simulates joint loading and allows the humerus to assume a self-aligned, “physiological” configuration [84].

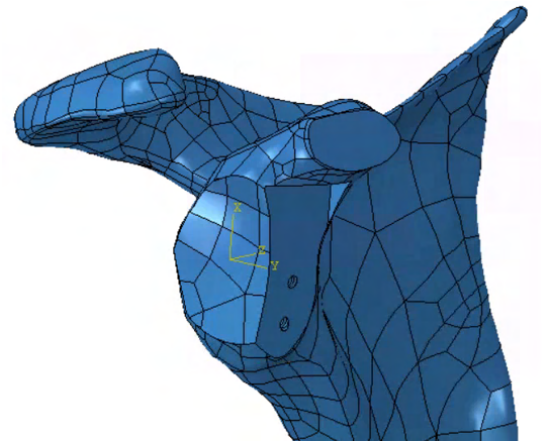

Figure 3.13: Coordinate System used for proper load and translation application. The x, y and z directions point in the superior, anterior and medial directions, respectively.

In step (2), the humeral head was translated in the anterior direction keeping permanent compression. Joint stability was considered compromised after peak translational shear force was reached, so a translation of 10 mm was considered sufficient to obtain the desired results [32]. Translational shear force refers to the force applied in the anterior direction necessary to obtain a certain displacement value in that same direction. As an anterior translation was applied to the center of the humeral head, the translational shear force was measured as the y component of the reaction force present at the center of the humeral head, during each frame of displacement.

3.2.4 Mesh

Due to the complex geometry of the structures, quadratic tetrahedral (C3D10) elements were used to create the FE meshes of the different modeled components. To ensure numerical stabilty of the results, a convergence analysis was performed. A model of the healthy GH joint, using the intact scapula and soft tissues (before creation of the bone defect and Latarjet simulation), was considered for this purpose. The representation of this model is present in Figure 3.14. Variations in peak translational force of the humerus and Von Mises stress with average element size were recorded in four points of the scapula near the glenoid. The nodes of the scapula are identified as Node 1 to 4 in Figure 3.14.

Mesh density was increased successively by decreasing average element sizes of each component. For the glenoid and humeral head cartilages and labrum the average element sizes ranged from 3 mm to 0.8 mm, while for the scapula these ranged from 4 mm to 1.3 mm. The humeral head, as it is not in contact with the glenoid cartilage, labrum or bone graft directly, was meshed with a fixed element size of 2.5 mm. In these simulations, the scapula was modeled using a homogeneous material with a Young's modulus of 10.4 GPa, corresponding to the average bone properties [97], and Poisson's ratio of 0.3. The results of the mesh convergence analysis are present in Figure 3.15.

As seen in Figure 3.15c, increasing the FE mesh density from 391176 elements to 472294 elements produced a change of less than 1% in both the Von Mises stress at the chosen nodes and the peak translational force of the humeral head. Therefore, a mesh containing 391176 was considered to have

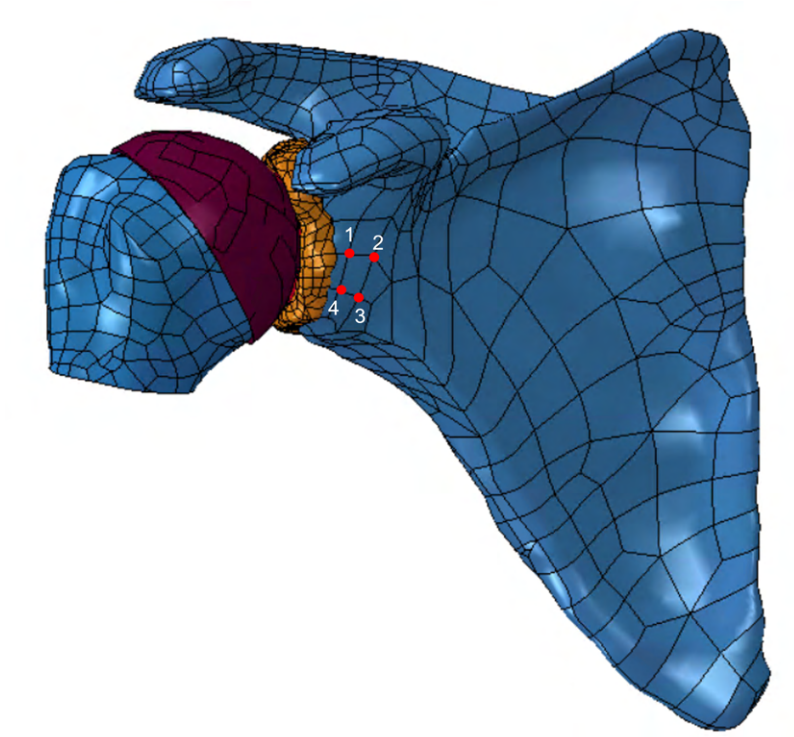

Figure 3.14: Anterior view of the healthy GH joint model with humerus in neutral position with identification of the nodes used for convergence analysis.

converged [33] and was selected for further use. The average element size of both the healthy and Latarjet model parts are summarized in Table 3.3.

Table 3.3: Mesh size and density of the different model components.

Model Part	Healthy Model		Latarjet Model	
	Av. El. Size (mm)	Nb of Elements	Av. El. Size (mm)	Nb of Elements
Humerus	2.5	22361	2.5	22361
Scapula	1.5	218827	1.5	233241
Labrum	0.8	52754	0.8	41589
Humeral Head Cartilage	0.8	81550	0.8	80639
Glenoid Cartilage	0.8	15684	0.8	16427
Bone Graft	-	-	0.5	27715
Cortex Screws	-	-	0.7	2054

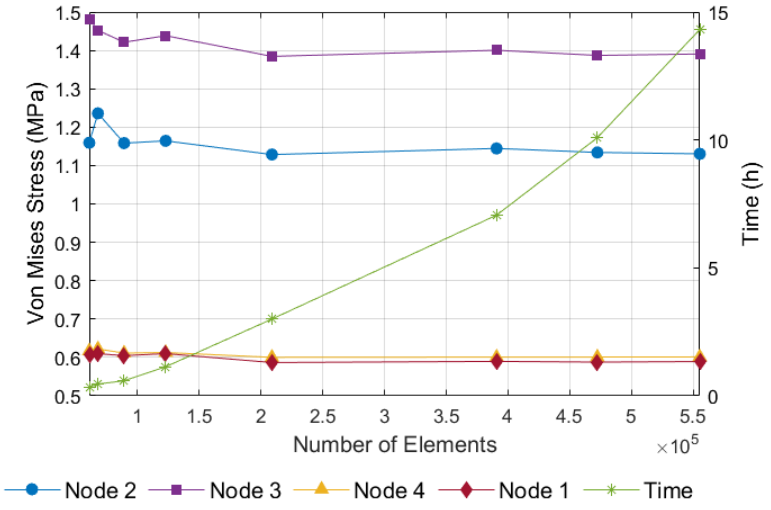

(a)

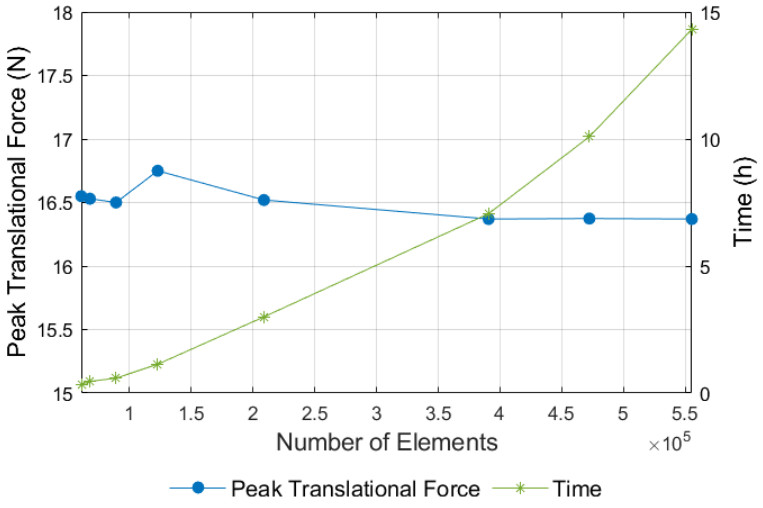

(b)

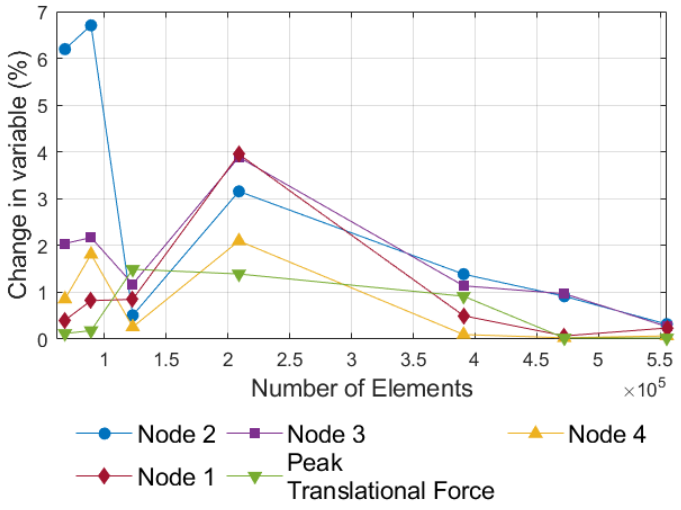

(c)

Figure 3.15: Mesh convergence analysis: (a) Evolution of Von Mises stress in Nodes 1-4 and computational time with mesh density; (b) Evolution of peak translational shear force of humeral head and computational time with mesh density; (c) Change in each variable relative to previous mesh.

3.3 Results Acquisition and Analysis

Using the conditions described in section 3.2, FE models were developed to reproduce different states of the GH joint. These encompass the healthy GH joint, the GH joint with glenoid bone defects and the GH joint following the Latarjet procedure.

The healthy GH joint model was used for validation, simulating the experimental procedure followed by Lippit et al. [30]. Similarly, the models of the GH joint, with glenoid bone defects of different sizes, were also used for validation, and, to this end, replicated the experimental procedure followed by Yamamoto et al. [8]. The models of the GH joint following the Latarjet procedure were used to evaluate the influence of graft position on shoulder stability and contact pressure.

This section presents the methods used for FE model validation and for analysis and comparison of the results.

3.3.1 Model Validation

The validation of the FE models developed consisted in estimating the joint stability and comparing the results with that reported in the literature. The stability of the joint was evaluated through the stability ratio (SR), which is defined as peak translational shear force divided by the applied compressive joint load:

$$\text{Stability Ratio } (SR) = \frac{\text{Peak Translational Force}}{\text{Compressive Force}} \tag{3.3}$$

For a healthy GH joint, Lippit et al. [30] translated the humeral head in 8 anatomic directions and calculated their respective SR. As this work focuses on anterior instability, the SR in the healthy GH joint model was only evaluated in the anterosuperior, anterior and anteroinferior directions. The anteroinferior and anterosuperior directions were defined at a 45° angle from the anterior direction in the XY plane, clockwise and anticlockwise, respectively.

For the GH joints with glenoid bone defects, the SR in the anterior direction, corresponding to each size of bone defect, was calculated and the results were compared to those of Yamamoto et al. [8], as this study performed the same analysis on cadaveric models.

As mentioned in section 3.2, contact stabilization was applied to some of the defined interactions. To ensure validity of the results, the maximum dissipated energy by stabilization was verified to be below 5% of the maximum internal energy of the model.

3.3.2 Comparison of Graft Position

To evaluate the effect of different graft positions, both the variation of stability of the joint and distribution of contact pressures in the humeral head cartilage were analyzed. The stability of the joint was computed using the SR for each graft position and arm position.

For comparison purposes, the contact pressures were taken only from the frames of the simulation

between the beginning of humeral head translation, when the humerus is at its physiological configuration, and achievement of maximum translational shear force. The displacement of the humeral head in the anterior direction was normalized with the former corresponding to 0 and the latter corresponding to 1. After peak translational shear force was reached, joint stability was considered to be compromised and the results were considered invalid for evaluating the effectiveness of the Latarjet procedure.

After appropriate selection and normalization of the results, the GH contact pressures were analyzed in qualitative and quantitative ways. Visual representations of contact pressure distribution in the glenoid cartilage, labrum and graft for the different graft positions were qualitatively examined and compared. These were represented at three frames: one corresponding to the initial frame of the analysis (beginning of humeral translation), one corresponding to a middle frame, and one corresponding to the last frame of the analysis (position at maximum shear force).

For a more objective evaluation, the values of contact pressure of each element in the humeral head surface were retrieved and its maximum and average at each displacement value were calculated. A script was developed in Matlab software to obtain the variation of peak contact pressure with humeral head displacement at the different modeled graft and arm positions.

Osteoarthritis risk was examined by comparison of peak GH contact pressures with the value of failure stress of cartilage. Peak GH contact pressures above the failure stress of cartilage were considered as a potential risk for the development of postoperative osteoarthritis as it could lead to cracking of the humeral head cartilage [98]. Due to lack of information regarding the mechanical failure of humeral head cartilage, the failure stress was approximated using the data published for the cartilage of the femoral head and for tensile failure [98], which is present in Figure 3.16.

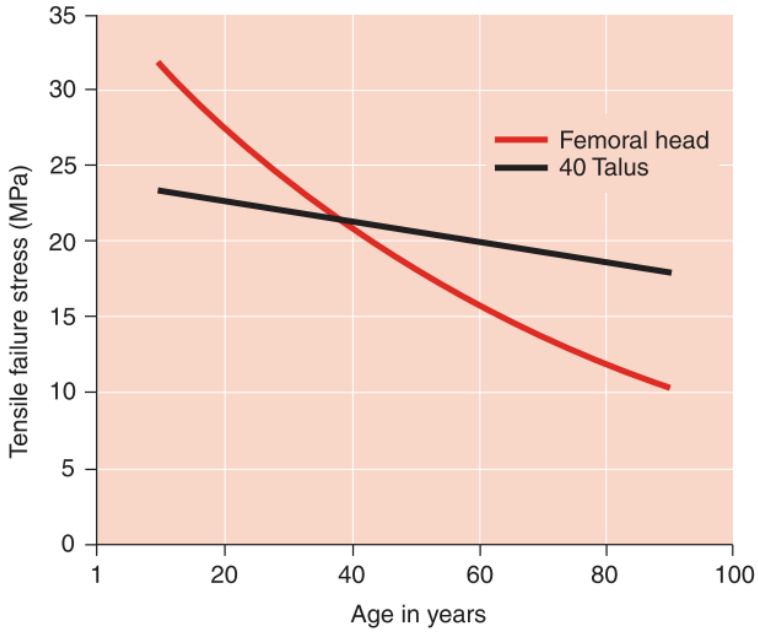

Figure 3.16: Comparison of the failure stress of cartilage from the hip and talus and their variation with age [98].

There is a significant drop in failure stress of the femoral head with age (Figure 3.16). As the Latarjet

procedure is performed more commonly in the young active population, as these constitute the majority of patients with anterior instability [2], the value of 25 MPa was chosen as the failure stress of cartilage for comparison with results of peak contact pressure.

The average contact pressure and contact area at each displacement value for each graft and arm position were also plotted.

Chapter 4

Results

This chapter presents the results obtained from the FE analyses, regarding both model validation and impact of graft position on joint stability and contact pressure.

4.1 Model Validation

The results for the SRs of the healthy model obtained in the 3 directions tested are present in Figure 4.1. Alongside these, the Figure also contains data of SRs achieved through cadaveric testing reported in the literature [30]. The values of SR are all in agreement with the published data.

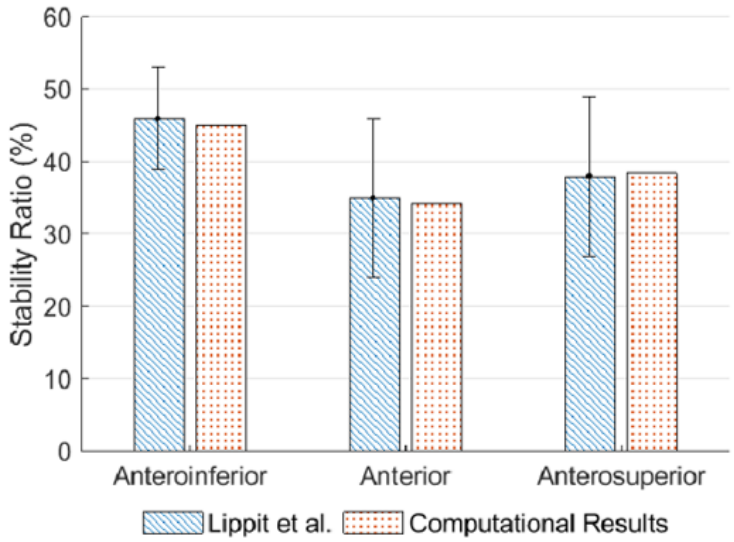

Figure 4.1: Stability Ratios of the GH joint in the anteroinferior, anterior and anterosuperior direction. Comparison with the mean and SD of stability ratios obtained by Lippit et al. [30].

The SRs for each bone defect size and their comparison with published data are illustrated in Figure 4.2. No change is observed between the results for defects of 8% and 14%, but all SRs still fall within standard deviation intervals published in the literature.

As mentioned in Section 3.2, the use of contact stabilization causes dissipation of energy. For all

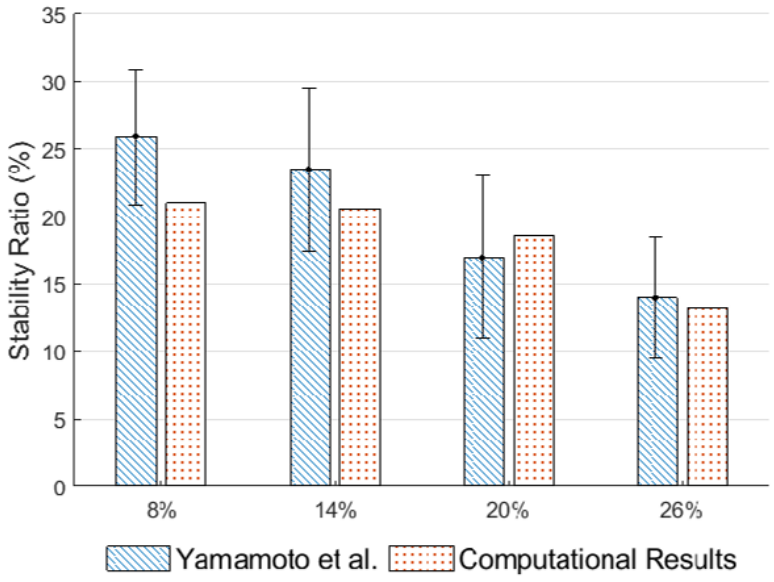

Figure 4.2: Stability Ratios of the GH joint with glenoid bone defects with a width representing 8%, 14%, 20% and 26% of glenoid height. Comparison with the mean and SD of stability ratios obtained by Yamamoto et al. [8].

simulations, the maximum dissipated energy was verified to be below 5% of the maximum internal energy. To exemplify the evolution of theses variables, Figure 4.3 shows the results of one energy analysis.

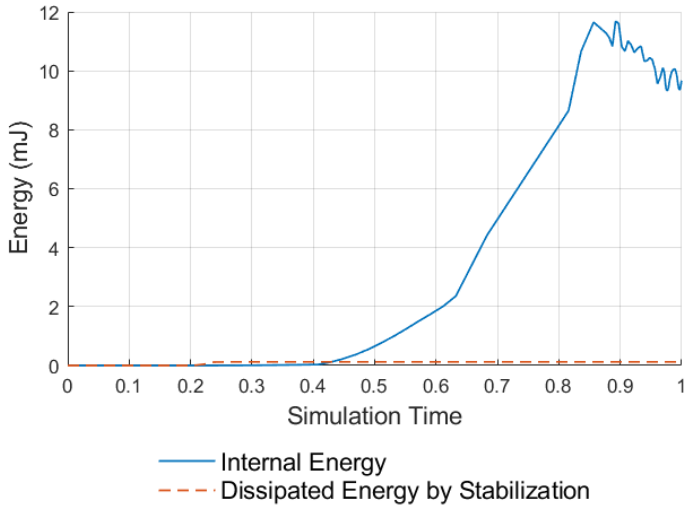

Figure 4.3: Comparison of Internal Energy of model and dissipated energy due to contact stabilization. Maximum dissipated energy corresponds to 1% of maximum internal energy.

4.2 Comparison of Graft Position

4.2.1 Stability Ratios

The SRs obtained for the anterior direction in all the modeled graft and arm positions are presented in Figure 4.4. Common to all arm positions, the SR rose with increasing laterality of the bone graft beyond the 1.5 mm position. No relevant difference is observed between stability of the reference and 1.5 mm models, regardless of humeral position.

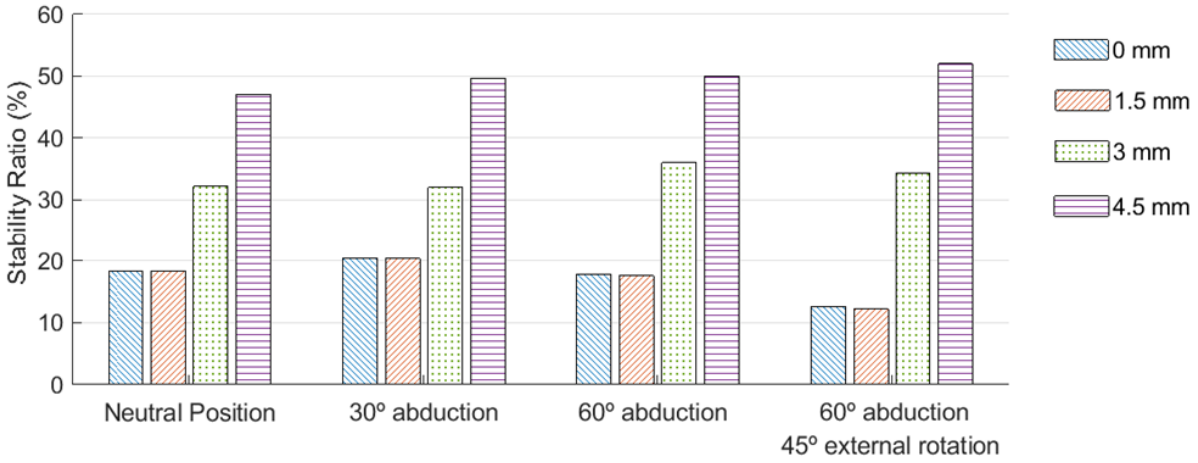

Figure 4.4: Comparison of stability Ratios of the GH joint after the Latarjet procedure for the modeled graft positions in each arm position.

The 3 mm model shows an average increase in SR of 16.5% from the 1.5 mm or reference models, while the 4.5 mm model's results increase, in average, 16% from the 3 mm ones. When comparing arm positions, the condition with 60° abduction and 45° external rotation shows the greatest variability in SR presenting both the lowest value in the 1.5 mm model and the highest one in the 4.5 mm model.

4.2.2 Contact Pressure Distribution

Figure 4.5 contains the contact pressure distribution in the glenoid cartilage, labrum and bone graft for the different graft positions at 60° GH abduction. For each graft position, 3 frames are shown, representing different displacement values of the humeral head. Changes observed between graft position are mostly similar for the various tested arm positions so the contact pressure distribution for the neutral, 30° abduction and 60° abduction with 45° external rotation are presented only in Appendix A.

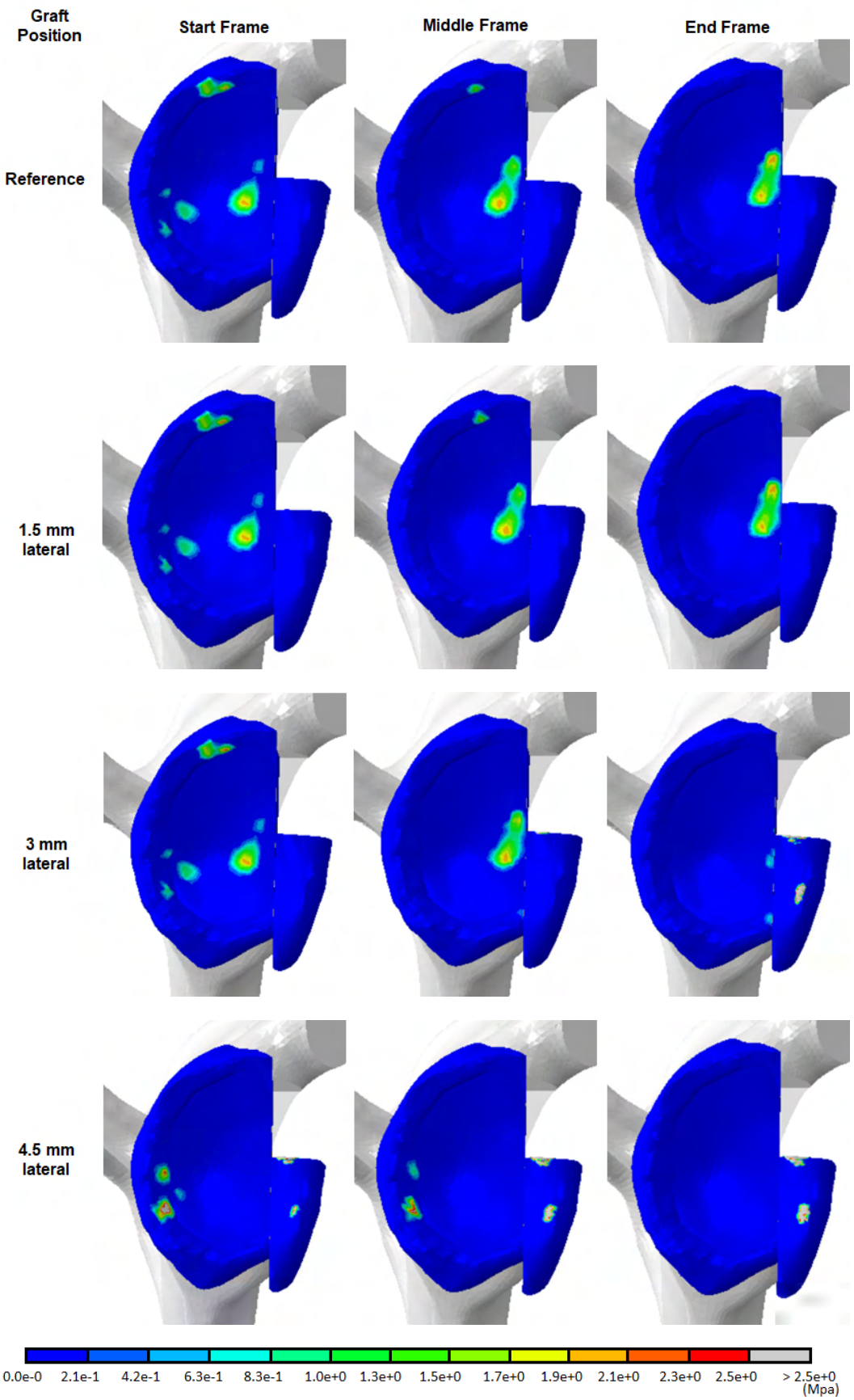

Figure 4.5: Start, middle and end frames of the simulation showing contact pressure distribution on the glenoid cartilage, labrum and bone graft for each graft position at 60° abduction. The start frame corresponds to the end of joint compression where humeral head translation is null. The end frame corresponds to the frame with maximum translational force.

The contact pressure distributions of the reference and 1.5 mm models are indistinguishable in every observed frame. At the start frame, when only a compressive force is present, the humeral head cartilage is in contact with both the glenoid cartilage and labrum. Contact in the labrum can be either more posterior or superior, depending on the position of the arm. The zone of contact in the glenoid cartilage moves anteriorly, accompanying the displacement of the humeral head. In both the reference and 1.5 mm models, the humeral head cartilage does not touch the bone graft for the entirety of the analyzed displacement interval.

For the 3 mm model, the initial contact distribution is similar to the previously described models; however, towards the end of the simulation the contact pressure is mostly present in the bone graft, showing magnitudes higher than the maximum observed for both reference and 1.5 mm models, represented by the gray areas. The 4.5 mm model has the majority of contact pressure distributed between only the glenoid labrum and bone graft, with the contact at the end frame being located only on the bone graft. Unlike for all other graft positions, the humeral head contacts the bone graft at the start of the simulation. Similarly to the 3 mm model, contact pressure values in the bone graft show high magnitude when compared to those in the cartilage and labrum.

For quantification and comparison of the evolution of contact pressure with anterior translation in the different graft positions, the displacement of the humeral head was normalized. The absolute displacement values from the physiological position (after application of only compressive force) to the position at maximum translation force in the anterior direction are shown in Table 4.1.

Table 4.1: Absolute displacement of humeral head from normal physiological placement in the glenoid until peak translational force in the different graft and arm positions.

Arm Position	Graft Position	Displacement (mm)
Neutral	Reference	1.9
	1.5 mm	1.9
	3 mm	3.7
	4.5 mm	2.0
30° abduction	Reference	1.6
	1.5 mm	1.6
	3 mm	4.7
	4.5 mm	1.6
60° abduction	Reference	1.7
	1.5 mm	1.7
	3 mm	4.2
	4.5 mm	1.1
60° abduction 45° external rotation	Reference	6.0
	1.5 mm	5.9
	3 mm	6.0
	4.5 mm	2.7

Progression of peak contact pressure of different bone graft models for each arm position studied can be observed in Figures 4.6, 4.7, 4.8 and 4.9. For every arm position, both the reference and 1.5 mm bone graft positions show similar results well below the threshold considered for the failure stress of cartilage. However, this threshold is consistently overrun when the graft is placed in a 3 mm or 4.5

mm lateral position. At the start frame, the 3 mm model shows peak pressures similar to models with a more medial graft position relative to it and only surpasses cartilage failure stress towards the end of the translation. On the other hand, the 4.5 mm model has a very high peak contact pressure at every displacement value, surpassing the stress threshold for the majority of the simulation.

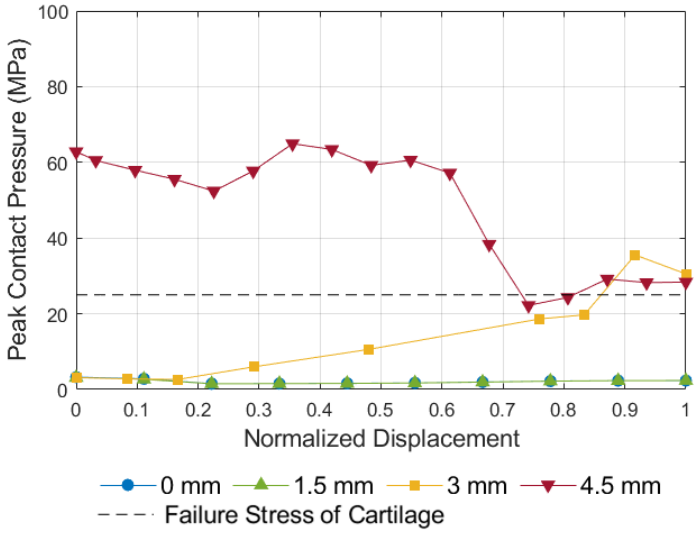

Figure 4.6: Evolution of peak contact pressure with normalized displacement of the humeral head for the different graft positions at the neutral position.

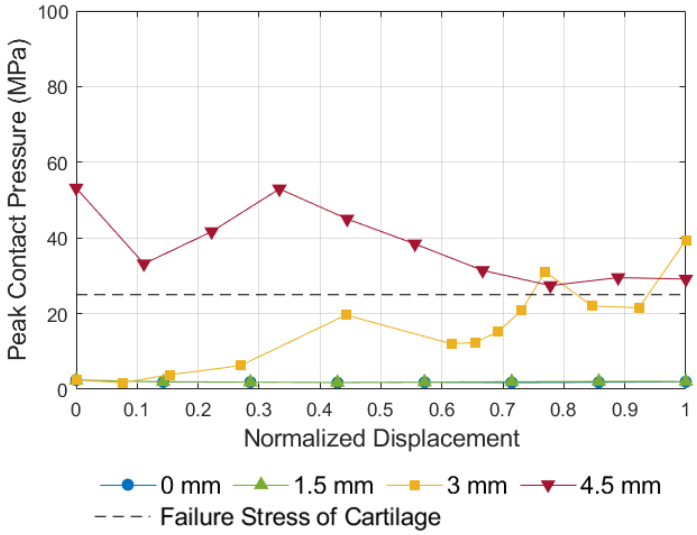

Figure 4.7: Evolution of peak contact pressure with normalized displacement of the humeral head for the different graft positions at 30° GH abduction.

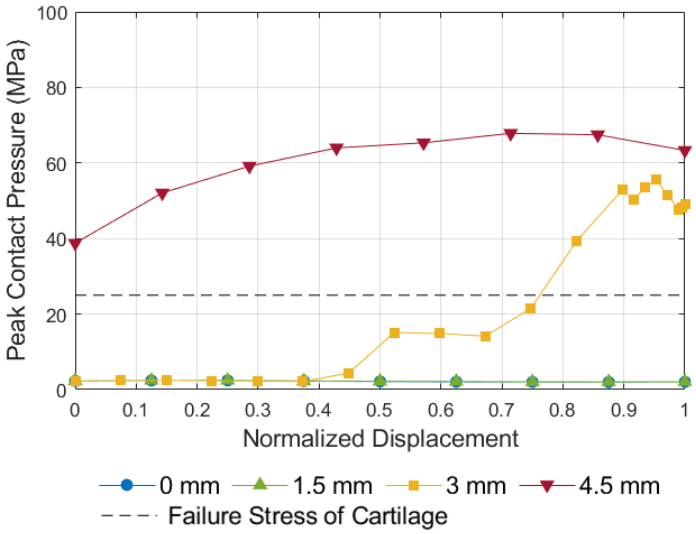

Figure 4.8: Evolution of peak contact pressure with normalized displacement of the humeral head for the different graft positions at 60° GH abduction.

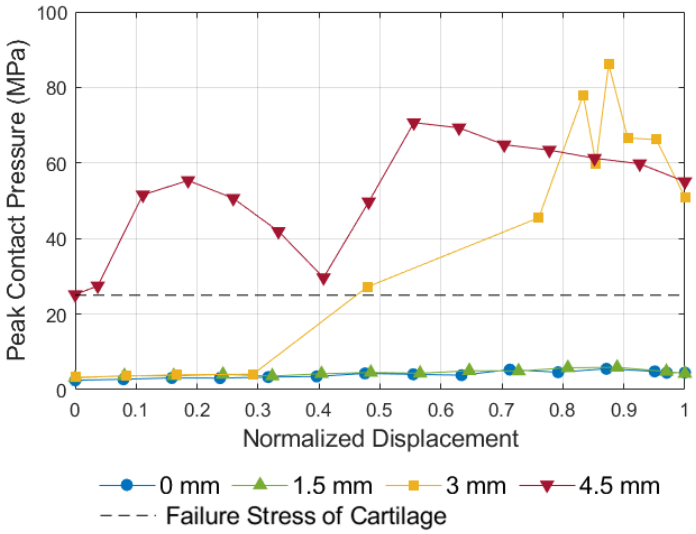

Figure 4.9: Evolution of peak contact pressure with normalized displacement of the humeral head for the different graft positions at 60° GH abduction with 45° external rotation.

When comparing arm positions, the biggest changes in peak contact pressure were observed for 60° abduction and 60° abduction with 45° external rotation. The latter shows the highest peak contact pressure values, which, unlike other arm positions occur for the 3 mm model and not the 4.5 mm one.

Changes in mean contact pressure with normalized displacement were also plotted. For the sake of brevity and due to similarities between most humeral positions, only the results for 60° GH abduction are presented in Figure 4.10. The results for the remaining arm positions can be consulted in Appendix B. Overall, the mean contact pressure seems to increase with anterior translation and with increasing lateral placement of the bone graft.

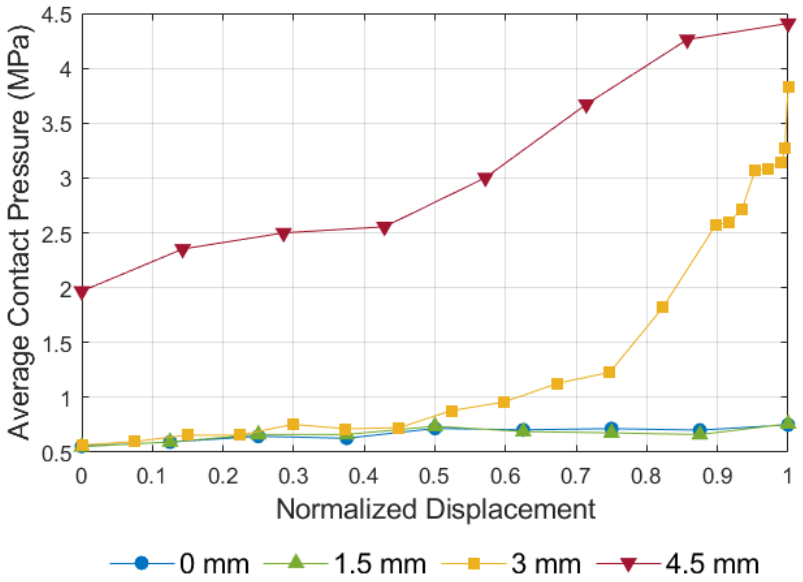

Figure 4.10: Evolution of mean contact pressure with normalized displacement of the humeral head for the different graft positions at 60° GH abduction.

Lastly, the contact area for each FE analysis was retrieved. The contact area over normalized displacement of each graft position for 60° GH abduction is presented in Figure 4.11. The information regarding the remaining arm positions is shown in Appendix C.

The contact area behaves opposite to the mean contact pressure by decreasing with anterior translation and with increasing lateral placement of the bone graft. The exception for this happens with the arm at 60° abduction and 45° external rotation, where a bone graft placed 4.5 mm lateral to the reference has a higher contact area at the start of the translation compared to all other graft positions.

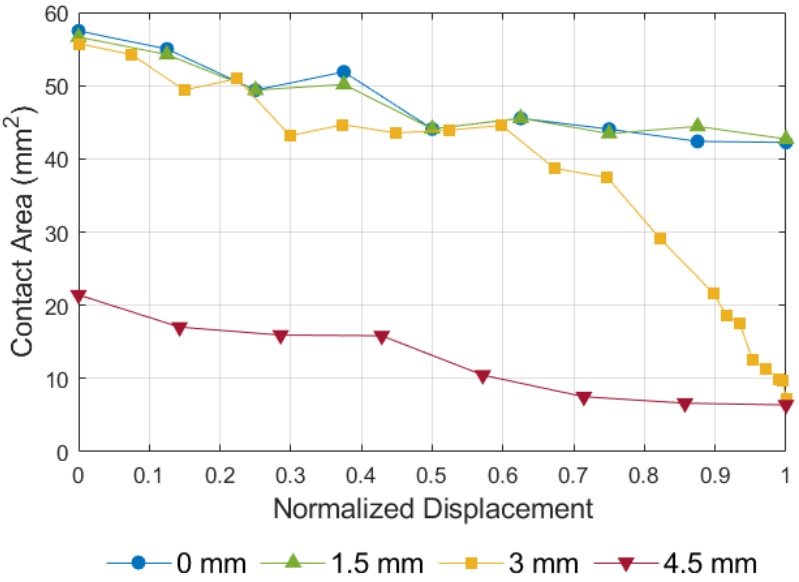

Figure 4.11: Evolution of GH contact area with normalized displacement of the humeral head for the different graft positions at 60° GH abduction.

Chapter 5

Discussion

5.1 Model Validation

The modelling of articular cartilage, labrum and bone defect geometries was validated against in vitro measurements of GH stability reported in the literature [30]. The SRs of the healthy GH joint model at the tested directions all fell within the literature ranges, which shows accuracy in the joint modeling of the soft tissues. When testing the stability of the bone defects, the results obtained were also within the standard deviation intervals measured in vitro. However, unlike the average measurements published, the SRs of the joint with 8% and 14% defects showed no variation between them. These results can be explained by the assumption of constant thickness in the glenoid cartilage. Differences in the thickness of this cartilage are more noticeable towards its exterior edges [26, 86], so when bigger glenoid bone defects are present this effect becomes less relevant. For simulation of the Latarjet procedure, a 20% bone defect was used, as it corresponds to the limit after which bone grafting procedures are recommended.

Both these validation processes provide confidence in the FE model of the GH joint and the results further obtained after simulation of the Latarjet procedure.

5.2 Comparison of graft position

The distribution of contact pressure over GH joint surfaces (Figure 4.5) provided insight into the role of the graft when placed in different positions. When the bone graft is placed in the reference or 1.5 mm lateral position, no contact between the humeral head cartilage and graft surface is observed for the entirety of the analysis. This translated to a low SR, showing no significant change between the two modeled positions. Adding to the resemblance of the results of both positions, their SR in the hanging arm position was also identical to that obtained for the model simulating the GH joint with a 20% bone defect before the Latarjet procedure was modeled. From these results, it can be concluded that placement of the graft in the reference and 1.5 mm lateral positions has a null contribution to the static stabilization of the GH joint in terms of osseous glenoid reconstruction, which can lead to an increased risk of recurrent instability.

Both the 3 mm and 4.5 mm graft positions showed contact between the bone graft and humeral head articular surface; however this contact occurred at different moments of humeral displacement. For the 3 mm model, initial contact pressure distribution was similar to the models with a more medially placed graft, which means that the humeral head had the same approximate physiological position. Contact with the bone graft occurred only towards the end of the humeral head translation, contributing to an increase in SR when compared to the 1.5 mm and reference models.

In the 4.5 mm model, due to the lateral overhang of the graft, the articulation of the humeral head became constrained, leading to a shift in contact surface in the posterior direction when submitted only to a compressive force. In this situation, the humeral head contacted with the graft at the start frame, unlike in all other positions, and reduced contact with the glenoid cartilage. The difference in joint alignment at a physiological position can pose an increased risk of osteoarthritis. The contact with the graft during only joint compression also leads to the decrease in anterior displacement of the humeral head until maximum translational force. A lateral overhanging of the graft, offers higher resistance to anterior translation of the humeral head, leading to an increase in SR. As the more lateral graft position studied, the 4.5 mm model presents the highest SR, with a value significantly higher than the SR of a health GH joint.

Observing the progression of peak contact pressure with displacement of the humeral head, it is noticeable that the 3 mm and 4.5 mm models systematically presented higher contact pressures. Both these models had peak contact pressures that surpassed the value representing the failure stress of cartilage, potentially leading to injuries in the humeral head cartilage related to the development of postoperative osteoarthritis [98]. The high values of contact pressure (above failure stress of cartilage) seem to be related to the contact between the humeral head cartilage and the bone graft. This is easily observable in the 3 mm model, as peak contact pressures had a significant increase towards the end of humeral head translation. The distribution of contact pressure on the bone graft had mostly two focal points, regardless of arm position, caused by the rough osseous incongruity of the lateral coracoid process surface. From thereon, much like Ghodara et al. [76] predicted, it can be concluded that the increase in contact pressure is caused by nonconformity of the contact surfaces in the classic Latarjet procedure.

Combining all previous remarks, the optimal position for placement of the bone graft during the Latarjet procedure is taken to be between the 1.5 mm and 3 mm positions modeled in this work. Although an exact placement could not be found, it still shortens the acceptable interval considered by many authors when evaluating surgical outcomes of the Latarjet procedure [17, 16, 15]. If the measurements of graft position obtained through the axial circle method, as reported in Table 3.1, are considered, the results obtained in this work are more easily comparable to those in the literature. The axial circle method was considered to better evaluate the graft position compared to the axial line method due to the irregular geometry of the graft. The interval found containing the optimal position of the bone graft was [-1.81, +0.44] mm in the medial lateral direction, with the zero being the circle fitted in the glenoid articular surface. This supports the recommendation of placing the coracoid graft as closely as possible flush to the glenoid surface.

The SR calculated support the belief that the osseous augmentation of the glenoid during the Latarjet procedure only contributes to stability through the glenoidplasty effect or reconstruction of the glenoid arc, agreeing with Yamamoto et al. [14]. This disregards the initial belief that the bone graft only needed to serve as a block to medial translation of the humerus. When the graft is placed medially to the glenoid face, the results are in accordance with Ghodadra et al. [76], suggesting that there is no reconstruction of the glenoid articular surface and no osseous block to anterior humeral translation during the different positions of arm abduction and external rotation.

As the 4.5 mm model is considered to be lateral to the glenoid surface, its contact pressure distribution presented in this work confirms the increase in posterior GH contact pressure and shift of the physiological humeral head position in the glenoid documented in the literature [76].

There are several limitations to this work. The first and foremost limitation is the lack of muscles and ligaments that participate in shoulder stabilization. The healthy shoulder stability model followed the setup of other studies [8, 30, 76] which do not take into account ligamentous or musculotendinous structures. For modeling the Latarjet procedure, the dynamic effect of the conjoint tendon was also neglected. The conjoint tendon of the short head of the biceps and coracobrachialis muscle originates from the tip of the coracoid process and plays a role in the stabilizing action of the Latarjet procedure. As discussed previously, it is responsible for the ”sling effect”, resisting anterior translation of the humerus and reinforcing the capsule by lowering the subscapularis (Figure 2.16). The sling behaviour of the conjoint tendon occurs during shoulder abduction, so the SR values obtained with abducted arm position could suffer changes if its effect was considered. However, even with the arm at 60° GH abduction and neutral external rotation, the effect of the osseous reconstruction of the glenoid has been reported to contribute up to 49% of the restored GH stability [14], so its importance cannot be neglected. For the arm positions modeled in this work, the bone effect of the Latarjet procedure still has a significant contribution for restoration of stability.

Lack of ligamentous structures, such as the GH capsule, can also cause variability within the results. An intact GH capsule could not only affect the SRs obtained but also prevent the posterior shift of GH contact pressures observed due to the lateral overhang of the bone graft. Nevertherless, the glenoid capsule is described as a lax structure in the hanging arm position [18]. Its significance for shoulder stability after performing the Latarjet procedure has been reported to be present in an end range position of abduction, with 60° GH abduction and maximum external rotation [14]. This signifies that some of the modeled positions are likely little affected by the absence of the GH capsule.

For the sake of comparison, the same load conditions were used for the validation processes and collection of results post Latarjet procedure. The load considered contained a small joint reaction force in magnitude and did not correspond to the range of in-vivo forces. The use of physiological load conditions could lead to some differences in GH contact pressure distribution and perhaps provide other relevant data.

Another limitation of this work was the use of a model of the same specimen and the same size of glenoid bone defect for all tested conditions of the Latarjet procedure. Variability in defect size and in graft width and height may affect change in stability and GH contact pressure. However, the present work

still demonstrated the effectiveness of glenoid reconstruction through the use of a bone graft collected from the coracoid process.

Chapter 6

Conclusions

The main objective of the present work was the assessment of the best position for bone graft placement during the Latarjet procedure. To achieve this, 3D FE models of the shoulder simulating the Latarjet procedure with different graft positions were developed and validated. Besides the different graft positions, to strengthen the validity of this work, the shoulder was modeled and tested at different positions of abduction and external rotation. Results were obtained through the evaluation of changes in joint stability and GH contact pressures caused by varying bone graft placement.

The best position for bone graft placement in the medio-lateral direction was found to be between two of the modeled positions, which were 1.5 mm and 3 mm lateral to the reference used in this work. Using the axial circle method for standardized measurements of the graft positions, the optimal interval corresponded to [-1.81, + 0.44] mm in the medio-lateral direction, with the zero being flush to the glenoid articular surface. The results also allowed for the drawing of the conclusion that values of contact pressure above those of the failure stress of cartilage were caused by contact with the rough incongruous geometry of the bone graft, which may lead to an increased risk in the development of post-operative osteoarthritis. Evaluation of joint stability yielded results consistent with published data, confirming that positions medial to the glenoid articular surface, bear no effect on the joint SR when compared to the model of a glenoid with a bone defect,since these do not reconstruct the articular arc. Overly lateral position of the graft can cause misalignment of the GH joint, a factor associated with osteoarthritis.

To the author's knowledge, this is the first study combining both stability and contact pressure distribution of the GH joint for assessment of optimal graft position in the Latarjet procedure. Although the findings of this work may give recommendations for improving the efficacy of the surgical technique, further studies are required to deepen the knowledge regarding this issue and address some of the limitations of this work. An important development would be the addition of the ligamentous and musculotendinous structures which participate in shoulder stabilization. One particular phenomenon which makes the Latarjet procedure popular is the addition of the sling effect provided by the conjoint tendon. Accounting for the influence of this structure and the joint capsule will supply relevant information about the restoration of stability in extreme ranges of motion. Regarding load application, this study mimicked the conditions employed for model validation; however, use of loading conditions simulating in-vivo situ-

ations should be further performed. For this work, anatomic information of only one subject was used, neglecting variability of the modeled structures. Although the geometry and properties were validated according to clinical data, further studies using a higher number of shoulder models would increase the validity of the results. Along with this, testing the application of the Latarjet procedure on different glenoid bone defect sizes should also present more clinically relevant data.

References

[1] B. Kazár and E. Relovszky. Prognosis of primary dislocation of the shoulder. *Acta Orthopaedica*, 40(2):216–224, 1969.

[2] M. A. Zacchilli and B. D. Owens. Epidemiology of shoulder dislocations presenting to emergency departments in the United States. *Journal of Bone and Joint Surgery - Series A*, 92(3):542–549, 2010.

[3] A. Pickett and S. Svoboda. Anterior Glenohumeral Instability. *Sports Medicine and Arthroscopy Review*, 25(3):156–162, 2017.

[4] E. J. Pope, J. P. Ward, and A. S. Rokito. Anterior shoulder instability: A history of arthroscopic treatment. *Bulletin of the NYU Hospital for Joint Diseases*, 69(1):44–49, 2011.

[5] A. W. Hasebroock, J. Brinkman, L. Foster, and J. P. Bowens. Management of primary anterior shoulder dislocations: a narrative review. *Sports Medicine - Open*, 5(1):31, 2019.

[6] A. S. Bankart. Recurrent or habitual dislocation of the shoulder-joint. *British Medical Journal*, 2 (3285):1132–1133, 1923.

[7] E. Itoi, S. B. Lee, L. J. Berglund, L. L. Berge, and K. N. An. The effect of a glenoid defect on anteroinferior stability of the shoulder after Bankart repair: A cadaveric study. *Journal of Bone and Joint Surgery - Series A*, 82(1):35–46, 2000.

[8] N. Yamamoto, E. Itoi, H. Abe, and K. Kikuchi. Effect of an Anterior Glenoid Defect on Anterior Shoulder Stability. *The American Journal of Sports Medicine*, 37(5):949–954, 2009.

[9] M. Latarjet. Treatment of recurrent dislocation of the shoulder. *Lyon Chir.*, 49:994–997, 1954.

[10] M. J. Griesser, J. D. Harris, B. W. McCoy, W. M. Hussain, M. H. Jones, J. Y. Bishop, and A. Miniaci. Complications and re-operations after Bristow-Latarjet shoulder stabilization: A systematic review. *Journal of Shoulder and Elbow Surgery*, 22(2):286–292, 2013.

[11] N. Mizuno, P. J. Denard, P. Raiss, B. Melis, and G. Walch. Long-term results of the Latarjet procedure for anterior instability of the shoulder. *Journal of Shoulder and Elbow Surgery*, 23(11): 1691–1699, 2014.

[12] J. Allain, D. Goutallier, and C. Glorion. Long-term results of the latarjet procedure for the treatment of anterior instability of the shoulder. *Journal of Bone and Joint Surgery - Series A*, 80(6):841–852, 1998.

[13] L. Hovelius, B. Sandström, A. Olofsson, O. Svensson, and H. Rahme. The effect of capsular repair, bone block healing, and position on the results of the Bristow-Latarjet procedure (study III): Long-term follow-up in 319 shoulders. *Journal of Shoulder and Elbow Surgery*, 21(5):647–660, 2012.

[14] N. Yamamoto, T. Muraki, K.-N. An, J. W. Sperling, R. H. Cofield, E. Itoi, G. Walch, and S. P. Steinmann. The Stabilizing Mechanism of the Latarjet Procedure. *The Journal of Bone and Joint Surgery*, 95(15):1390–1397, 2013.

[15] T. M. Kraus, N. Graveleau, Y. Bohu, E. Pansard, S. Klouche, and P. Hardy. Coracoid graft positioning in the Latarjet procedure. *Knee Surgery, Sports Traumatology, Arthroscopy*, 24(2):496–501, 2016.

[16] J. Barth, L. Neyton, P. Métais, J. C. Panisset, L. Baverel, G. Walch, and L. Lafosse. Is the two-dimensional computed tomography scan analysis reliable for coracoid graft positioning in Latarjet procedures? *Journal of Shoulder and Elbow Surgery*, 26(8):e237–e242, 2017.

[17] J. Kany, O. Flamand, J. Grimberg, R. Guinand, P. Croutzet, R. Amaravathi, and P. Sekaran. Arthroscopic Latarjet procedure: Is optimal positioning of the bone block and screws possible? A prospective computed tomography scan analysis. *Journal of Shoulder and Elbow Surgery*, 25(1):69–77, 2016.

[18] G. C. Terry and T. M. Chopp. Functional Anatomy of the Shoulder. *Journal of Athletic Training*, 35 (3):248–255, 2000.

[19] G. J. Tortora and B. Derrickson. *Introduction to the Human Body: the essentials of anatomy and physiology*. John Wiley & Sons, Inc, 8th edition, 2010.

[20] F. H. Netter. *Atlas of Human Anatomy*. Netter Basic Science. Elsevier, 7th edition, 2018.

[21] W. B. Kibler. The role of the scapula in athletic shoulder function. *American Journal of Sports Medicine*, 26(2):325–337, 1998.

[22] A. Agur, A. Dalley, and K. Moore. *Clinically oriented anatomy*. Wolters Kluwer Health/Lippincott Williams & Wilkins, 7th edition, 2014.

[23] Bones of the pectoral girdle and upper limb (illustrations). `https://radiopaedia.org/cases/bones-of-the-pectoral-girdle-and-upper-limb-illustrations?lang=us` [available online; accessed 16 October 2021].

[24] H. E. Veeger and F. C. van der Helm. Shoulder function: The perfect compromise between mobility and stability. *Journal of Biomechanics*, 40(10):2119–2129, 2007.

[25] L. C. Abbott and D. B. Lucas. The function of the clavicle; its surgical significance. *Annals of surgery*, 140(4):583–599, 1954.

[26] L. J. Soslowsky, E. L. Flatow, L. U. Bigliani, and V. C. Mow. Articular geometry of the glenohumeral joint. *Clinical Orthopaedics and Related Research*, (285):181–190, 1992.

[27] A. Deutsch, D. W. Altchek, E. Schwartz, J. Otis, and R. Warren. Radiologic measurement of superior displacement of the humeral head in the impingement syndrome. *Journal of shoulder and elbow surgery*, 5(3):186–193, 1996.

[28] N. K. Poppen and P. Walker. Normal and abnormal motion of the shoulder. *The Journal of Bone & Joint Surgery*, 3(2):195–201, 1976.

[29] K. E. Wilk, C. A. Arrigo, and J. R. Andrews. Current concepts: The stabilizing structures of the glenohumeral joint. *Journal of Orthopaedic and Sports Physical Therapy*, 25(6):364–379, 1997.

[30] S. B. Lippitt, J. E. Vanderhooft, S. L. Harris, J. A. Sidles, D. T. Harryman, and F. A. Matsen. Glenohumeral stability from concavity-compression: A quantitative analysis. *Journal of Shoulder and Elbow Surgery*, 2(1):27–35, 1993.

[31] S. M. Howell and B. J. Galinat. The glenoid-labral socket: A constrained articular surface. *Clinical Orthopaedics and Related Research*, (243):122–125, 1989.

[32] A. M. Halder, S. G. Kuhl, M. E. Zobitz, D. Larson, and K.-N. An. Effects of the Glenoid Labrum and Glenohumeral Abduction on Stability of the Shoulder Joint. *The Journal of Bone and Joint Surgery*, 83-A(7):1062–1069, 2001.

[33] C. Klemt, D. Nolte, G. Grigoriadis, E. Di Federico, P. Reilly, and A. M. Bull. The contribution of the glenoid labrum to glenohumeral stability under physiological joint loading using finite element analysis. *Computer Methods in Biomechanics and Biomedical Engineering*, 20(15):1613–1622, 2017.

[34] H. Gray. *Gray's Anatomy*. 20th edition, 1918.

[35] W. Bakhsh and G. Nicandri. Anatomy and Physical Examination of the Shoulder. *Sports Medicine and Arthroscopy Review*, 26(3):e10–e22, 2018.

[36] J. B. Myers and S. M. Lephart. The Role of the Sensorimotor System in the Athletic Shoulder. *Journal of Athletic Training*, 35(3):351–363, 2000.

[37] C. Rockwood, M. Wirth, F. Matsen, S. Lippitt, and J. Sperling. *Rockwood and Matsen's the Shoulder*. Elsevier, 2016.

[38] K. Krøner, T. Lind, and J. Jensen. The epidemiology of shoulder dislocations. *Archives of Orthopaedic and Trauma Surgery*, 108(5):288–290, 1989.

[39] A. Nordqvist and C. J. Petersson. Incidence and causes of shoulder girdle injuries in an urban population. *Journal of Shoulder and Elbow Surgery*, 4(2):107–112, 1995.

[40] S. Liavaag, S. Svenningsen, O. Reikerås, M. Enger, T. Fjalestad, A. H. Pripp, and J. I. Brox. The epidemiology of shoulder dislocations in Oslo. *Scandinavian Journal of Medicine and Science in Sports*, 21(6):e344–e340, 2011.

[41] A. Shah, A. Judge, A. Delmestri, K. Edwards, N. K. Arden, D. Prieto-Alhambra, T. A. Holt, R. A. Pinedo-Villanueva, S. Hopewell, S. E. Lamb, A. Rangan, A. J. Carr, G. S. Collins, and J. L. Rees. Incidence of shoulder dislocations in the UK, 1995-2015: A population-based cohort study. *BMJ Open*, 7(11):e016112, 2017.

[42] H. L. McLaughlin and W. U. Cavallaro. Primary anterior dislocation of the shoulder. *The American Journal of Surgery*, 80(6):615–621, 1950.

[43] G. E. Antonio, J. F. Griffith, A. B. Yu, P. S. Yung, M. C. Kai, and A. T. Ahuja. First-time shoulder dislocation: High prevalence of labral injury and age-related differences revealed by MR arthrography. *Journal of Magnetic Resonance Imaging*, 26(4):983–991, 2007.

[44] K. Horst, R. Von Harten, C. Weber, H. Andruszkow, R. Pfeifer, T. Dienstknecht, and H. C. Pape. Assessment of coincidence and defect sizes in Bankart and Hill-Sachs lesions after anterior shoulder dislocation: A radiological study. *British Journal of Radiology*, 87(1034), 2014.

[45] C. K. Yiannakopoulos, E. Mataragas, and E. Antonogiannakis. A Comparison of the Spectrum of Intra-articular Lesions in Acute and Chronic Anterior Shoulder Instability. *Arthroscopy - Journal of Arthroscopic and Related Surgery*, 23(9):985–990, 2007.

[46] D. S. Kim, Y. S. Yoon, and Chang Ho Yi. Prevalence comparison of accompanying lesions between primary and recurrent anterior dislocation in the shoulder. *American Journal of Sports Medicine*, 38(10):2071–2076, 2010.

[47] B. Zacharia, A. Prakas, S. Vaidyanathan, A. Roy, and M. K. Ayyub. The Shoulder Instability: An Overview. *International Journal of Recent Surgical and Medical Sciences*, (eFirst), 2021.

[48] H. Saito, E. Itoi, H. Sugaya, H. Minagawa, N. Yamamoto, and Y. Tuoheti. Location of the glenoid defect in shoulders with recurrent anterior dislocation. *American Journal of Sports Medicine*, 33(6): 889–893, 2005.

[49] J. F. Griffith, G. E. Antonio, C. W. Tong, and C. K. Ming. Anterior shoulder dislocation: Quantification of glenoid bone loss with CT. *American Journal of Roentgenology*, 180(5):1423–1430, 2003.

[50] S. S. Burkhart and J. F. De Beer. Traumatic glenohumeral bone defects and their relationship to failure of arthroscopic Bankart repairs: Significance of the inverted-pear glenoid and the humeral engaging Hill-Sachs lesion. *Arthroscopy: The Journal of Arthroscopic and Related Surgery*, 16(7): 677–694, 2000.

[51] P. E. Greis, M. G. Scuderi, A. Mohr, K. N. Bachus, and R. T. Burks. Glenohumeral articular contact areas and pressures following labral and osseous injury to the anteroinferior quadrant of the glenoid. *Journal of Shoulder and Elbow Surgery*, 11(5):442–451, 2002.

[52] P. Walia, A. Miniaci, M. H. Jones, and S. D. Fening. Influence of Combined Hill-Sachs and Bony Bankart Defects on Range of Motion in Anterior Instability of the Shoulder in a Finite Element Model. *Arthroscopy - Journal of Arthroscopic and Related Surgery*, 31(11):2119–2127, 2015.

[53] T. Pevny, R. E. Hunter, and J. R. Freeman. Primary traumatic anterior shoulder dislocation in patients 40 years of age and older. *Arthroscopy*, 14(3):289–294, 1998.

[54] R. Berbig, D. Weishaupt, J. Prim, and O. Shahin. Primary anterior shoulder dislocation and rotator cuff tears. *Journal of Shoulder and Elbow Surgery*, 8(3):220–225, 1999.

[55] K. Hayes, M. Callanan, J. Walton, A. Paxinos, and G. A. C. Murrell. Shoulder Instability: Management and Rehabilitation. *Journal of Orthopaedic & Sports Physical Therapy*, 32(10):497–509, 2002.

[56] C. J. Fedorka and M. K. Mulcahey. Recurrent anterior shoulder instability: A review of the Latarjet procedure and its postoperative rehabilitation. *Physician and Sportsmedicine*, 43(1):73–79, 2015.

[57] J. H. Wheeler, J. B. Ryan, R. A. Arciero, and R. N. Molinari. Arthroscopic versus nonoperative treatment of acute shoulder dislocations in young athletes. *Arthroscopy: The Journal of Arthroscopic and Related Surgery*, 5(3):213–217, 1989.

[58] I. Gigis, R. Heikenfeld, A. Kapinas, R. Listringhaus, and G. Godolias. Arthroscopic versus conservative treatment of first anterior dislocation of the shoulder in adolescents. *Journal of Pediatric Orthopaedics*, 34(4):421–425, 2014.

[59] F. S. Kralinger, K. Golser, R. Wischatta, M. Wambacher, and G. Sperner. Predicting recurrence after primary anterior shoulder dislocation. *American Journal of Sports Medicine*, 30(1):116–120, 2002.

[60] R. H. Brophy and R. G. Marx. The Treatment of Traumatic Anterior Instability of the Shoulder: Nonoperative and Surgical Treatment, 2009.

[61] C. Klemt. *Musculoskeletal Shoulder Modelling for Clinical Applications*. PhD thesis, 2018.

[62] W. EM and A. A. Hill-Sachs remplissage, an arthroscopic solution for the engaging Hill-Sachs lesion: 2- to 10-year follow-up and incidence of recurrence. *Journal of shoulder and elbow surgery*, 23(6):814–820, 2014.

[63] A. Novoa-Boldo and L. V. Gulotta. Expectations Following Rotator Cuff Surgery. *Current Reviews in Musculoskeletal Medicine*, 11(1):162–166, 2018.

[64] I. Elkinson, J. W. Giles, K. J. Faber, H. W. Boons, L. M. Ferreira, J. A. Johnson, and G. S. Athwal. The effect of the remplissage procedure on shoulder stability and range of motion: An in vitro biomechanical assessment. *Journal of Bone and Joint Surgery - Series A*, 94(11):1003–1012, 2012.

[65] S. Bhatia, R. M. Frank, N. S. Ghodadra, A. R. Hsu, A. A. Romeo, B. R. Bach, P. Boileau, and M. T. Provencher. The outcomes and surgical techniques of the Latarjet procedure. *Arthroscopy - Journal of Arthroscopic and Related Surgery*, 30(2):227–235, 2014.

[66] L. Lafosse, E. Lejeune, A. Bouchard, C. Kakuda, R. Gobezie, and T. Kochhar. The Arthroscopic Latarjet Procedure for the Treatment of Anterior Shoulder Instability. *Arthroscopy - Journal of Arthroscopic and Related Surgery*, 23(11):1242.e1–1242.e5, 2007.

[67] B. Altintas, J. A. Godin, and P. J. Millett. Anterior Instability with Bone Loss: Latarjet Procedure. In *Advanced Techniques in Shoulder Arthroscopy*, pages 131–139. Springer, Cham, 2019.

[68] D. Patte, B. J, and P. Bancel. The anteroinferior vulnerable point of the glenoid rim. In J. E. Bateman and R. P. Welsh, editors, *Surgery of the Shoulder*, pages p 94–99. New York: Dekker, 1985.

[69] G. Di Giacomo, A. Costantini, N. De Gasperis, A. De Vita, B. K. Lin, M. Francone, M. A. Rojas Beccaglia, and M. Mastantuono. Coracoid graft osteolysis after the Latarjet procedure for anteroinferior shoulder instability: a computed tomography scan study of twenty-six patients. *Journal of Shoulder and Elbow Surgery*, 20(6):989–995, 2011.

[70] S. S. Burkhart, J. F. De Beer, J. R. Barth, T. Criswell, C. Roberts, and D. P. Richards. Results of Modified Latarjet Reconstruction in Patients With Anteroinferior Instability and Significant Bone Loss. *Arthroscopy - Journal of Arthroscopic and Related Surgery*, 23(10):1033–1041, 2007.

[71] P. Domos, E. Lunini, and G. Walch. Contraindications and complications of the Latarjet procedure. *Shoulder and Elbow*, 10(1):15–24, 2018.

[72] H. Sano, T. Komatsuda, H. Abe, H. Ozawa, and T. A. Yokobori. Proximal-medial part in the coracoid graft demonstrates the most evident stress shielding following the Latarjet procedure: a simulation study using the 3-dimensional finite element method. *Journal of Shoulder and Elbow Surgery*, 29 (12):2632–2639, 2020.

[73] D. L. Haeni, G. Opsomer, A. Sood, J. Munji, M. Sanchez, B. Villain, G. Walch, and L. Lafosse. Three-dimensional volume measurement of coracoid graft osteolysis after arthroscopic Latarjet procedure. *Journal of Shoulder and Elbow Surgery*, 26(3):484–489, 2017.

[74] Y. M. Zhu, C. Y. Jiang, Y. Lu, F. L. Li, and G. Wu. Coracoid bone graft resorption after Latarjet procedure is underestimated: A new classification system and a clinical review with computed tomography evaluation. *Journal of Shoulder and Elbow Surgery*, 24(11):1782–1788, 2015.

[75] N. B. Alp, O. Doğan, T. G. Yılmaz, O. C. Kalay, A. A. Moussa, F. Karpat, M. Khandaker, and G. Akdag. Understanding the causes behind coracoid graft osteolysıs in latarjet procedure (finite element analysis and comparison of three fixation methods). *Orthopaedics and Traumatology: Surgery and Research*, 106(1):53–59, 2020.

[76] N. Ghodadra, A. Gupta, A. A. Romeo, B. R. Bach, N. Verma, E. Shewman, J. Goldstein, and M. T. Provencher. Normalization of glenohumeral articular contact pressures after Latarjet or iliac crest bone-grafting. *Journal of Bone and Joint Surgery - Series A*, 92(6):1478–1489, 2010.

[77] N. Yamamoto, T. Muraki, J. W. Sperling, S. P. Steinmann, R. H. Cofield, E. Itoi, and K.-N. An. Stabilizing Mechanism in Bone-Grafting of a Large Glenoid Defect. *Journal of Bone and Joint Surgery*, 92(11):2059–2066, 2010.

[78] L. Neyton, J. Barth, G. Nourissat, P. Métais, P. Boileau, G. Walch, and L. Lafosse. Arthroscopic Latarjet Techniques: Graft and Fixation Positioning Assessed With 2-Dimensional Computed Tomography Is Not Equivalent With Standard Open Technique. *Arthroscopy - Journal of Arthroscopic and Related Surgery*, 34(7):2032–2040, 2018.

[79] J. Beer, S. S. Burkhart, C. P. Roberts, K. Van Rooyen, T. Cresswell, and D. F. Du Toit. The congruent-arc Latarjet. *Techniques in Shoulder and Elbow Surgery*, 10(2):62–67, 2009.

[80] S. R. Montgomery, J. C. Katthagen, J. D. Mikula, D. C. Marchetti, D. S. Tahal, G. J. Dornan, K. D. Dahl, A. W. Brady, T. L. Turnbull, and P. J. Millett. Anatomic and Biomechanical Comparison of the Classic and Congruent-Arc Techniques of the Latarjet Procedure. *American Journal of Sports Medicine*, 45(6):1252–1260, 2017.

[81] C. Quental, J. Folgado, J. Ambrósio, and J. Monteiro. A multibody biomechanical model of the upper limb including the shoulder girdle. *Multibody System Dynamics 2012 28:1*, 28(1):83–108, 2012.

[82] C. Quental, J. Folgado, P. R. Fernandes, and J. Monteiro. Computational analysis of polyethylene wear in anatomical and reverse shoulder prostheses. *Medical and Biological Engineering and Computing*, 53(2):111–122, 2015.

[83] A. J. Sophia Fox, A. Bedi, and S. A. Rodeo. The basic science of articular cartilage: Structure, composition, and function. *Sports Health*, 1(6):461–468, 2009.

[84] P. Favre, M. Senteler, J. Hipp, S. Scherrer, C. Gerber, and J. G. Snedeker. An integrated model of active glenohumeral stability. *Journal of Biomechanics*, 45(13):2248–2255, 2012.

[85] J. A. Fox, B. J. Cole, A. A. Romeo, A. K. Meininger, J. M. Williams, R. E. Glenn, J. Bicos, J. K. Hayden, and C. B. Dorow. Articular cartilage thickness of the humeral head: An anatomic study. *Orthopedics*, 31(3), 2008.

[86] L. R. Yeh, S. Kwak, Y. S. Kim, D. S. Chou, C. Muhle, A. Skaf, D. Trudell, and D. Resnick. Evaluation of articular cartilage thickness of the humeral head and the glenoid fossa by MR arthrography: Anatomic correlation in cadavers. *Skeletal Radiology*, 27(9):500–504, 1998.

[87] J. Wermers, B. Schliemann, M. J. Raschke, P. A. Michel, L. F. Heilmann, F. Dyrna, J. Sußiek, A. Frank, and J. C. Katthagen. Glenoid concavity has a higher impact on shoulder stability than the size of a bony defect. *Knee Surgery, Sports Traumatology, Arthroscopy*, 2021.

[88] C. D. Bryce, A. C. Davison, G. S. Lewis, L. Wang, D. J. Flemming, and A. D. Armstrong. Two-dimensional glenoid version measurements vary with coronal and sagittal scapular rotation. *Journal of Bone and Joint Surgery - Series A*, 92(3):692–699, 2010.

[89] G. Wu, F. C. Van Der Helm, H. E. Veeger, M. Makhsous, P. Van Roy, C. Anglin, J. Nagels, A. R. Karduna, K. McQuade, X. Wang, F. W. Werner, and B. Buchholz. ISB recommendation on definitions of joint coordinate systems of various joints for the reporting of human joint motion - Part II: Shoulder, elbow, wrist and hand. *Journal of Biomechanics*, 38(5):981–992, 2005.

[90] A. Terrier, A. Reist, A. Vogel, and A. Farron. Effect of supraspinatus deficiency on humerus translation and glenohumeral contact force during abduction. *Clinical Biomechanics*, 22(6):645–651, 2007.

[91] S. Gupta and P. Dan. Bone geometry and mechanical properties of the human scapula using computed tomography data. *Trends Biomater Artif Organs*, 17(2):61–70, 2004.

[92] N. K. Knowles, G. D. G. Langohr, M. Faieghi, A. J. Nelson, and L. M. Ferreira. A comparison of density–modulus relationships used in finite element modeling of the shoulder. *Medical Engineering and Physics*, 66:40–46, 2019.

[93] W. Pomwenger, K. Entacher, H. Resch, and P. Schuller-Götzburg. Need for CT-based bone density modelling in finite element analysis of a shoulder arthroplasty revealed through a novel method for result analysis. *Biomedizinische Technik*, 59(5):421–430, 2014.

[94] C. Quental, J. Folgado, P. R. Fernandes, and J. Monteiro. Subject-specific bone remodelling of the scapula. *Computer Methods in Biomechanics and Biomedical Engineering*, 17(10):1129–1143, 2014.

[95] C. D. Smith, S. D. Masouros, A. M. Hill, A. L. Wallace, A. A. Amis, and A. M. Bull. The Compressive Behavior of the Human Glenoid Labrum May Explain the Common Patterns of SLAP Lesions. *Arthroscopy - Journal of Arthroscopic and Related Surgery*, 25(5):504–509, 2009.

[96] P. Buchler, N. A. Ramaniraka, L. R. Rakotomanana, J. P. Iannotti, and A. Farron. A finite element model of the shoulder : application to the comparison of normal and osteoarthritic joints. *Clinical Biomechanics*, 17:630–639, 2002.

[97] B. Helgason, F. Taddei, H. Pálsson, E. Schileo, L. Cristofolini, M. Viceconti, and S. Brynjólfsson. A modified method for assigning material properties to FE models of bones. *Medical Engineering and Physics*, 30(4):444–453, 2008.

[98] J. M. Mansour. Biomechanics of cartilage. In *Kinesiology: The Mechanics and Pathomechanics of Human Movement: Second Edition*, chapter 5, pages 69–83. Walters Kluwer Health, 2nd edition, 2013.

Appendix A

Contact Pressure Distribution

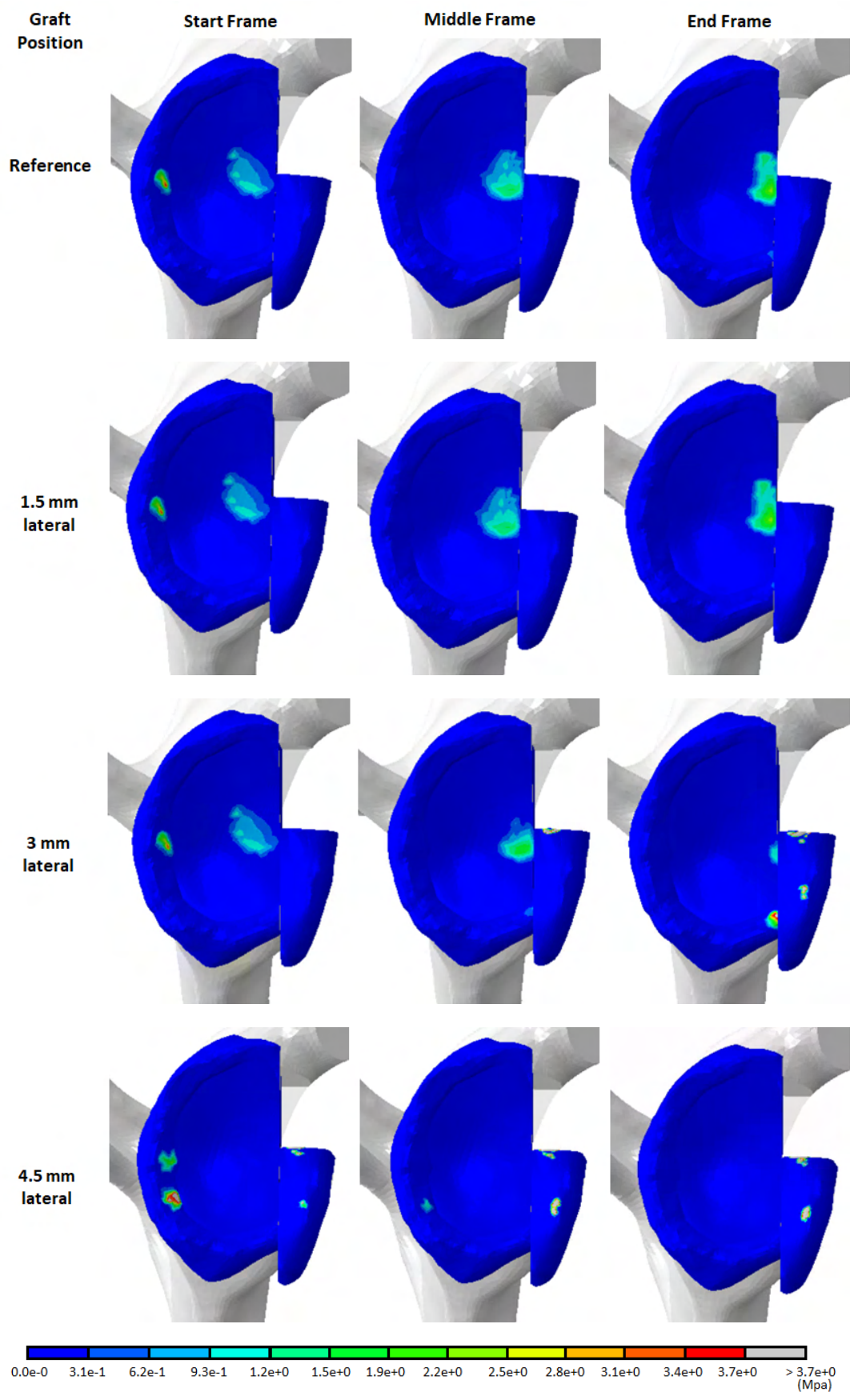

Figure A.1: Start, middle and end frames of the simulation showing contact pressure distribution on the glenoid cartilage, labrum and bone graft for each graft position at neutral humeral head position. The start frame corresponds to the end of joint compression where humeral head translation is null. The end frame corresponds to the frame with maximum translational force.

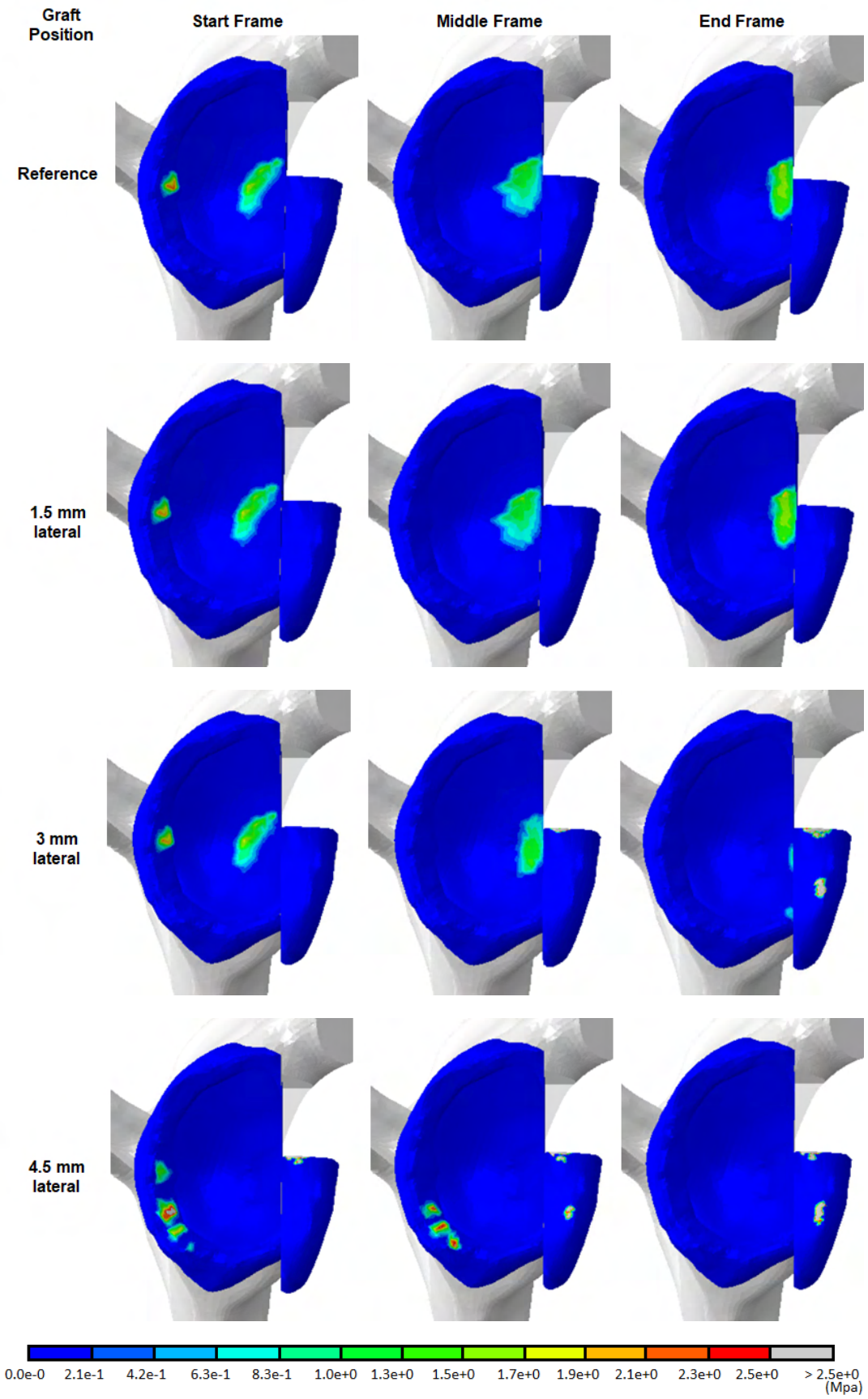

Figure A.2: Start, middle and end frames of the simulation showing contact pressure distribution on the glenoid cartilage, labrum and bone graft for each graft position at 30° abduction. The start frame corresponds to the end of joint compression where humeral head translation is null. The end frame corresponds to the frame with maximum translational force.

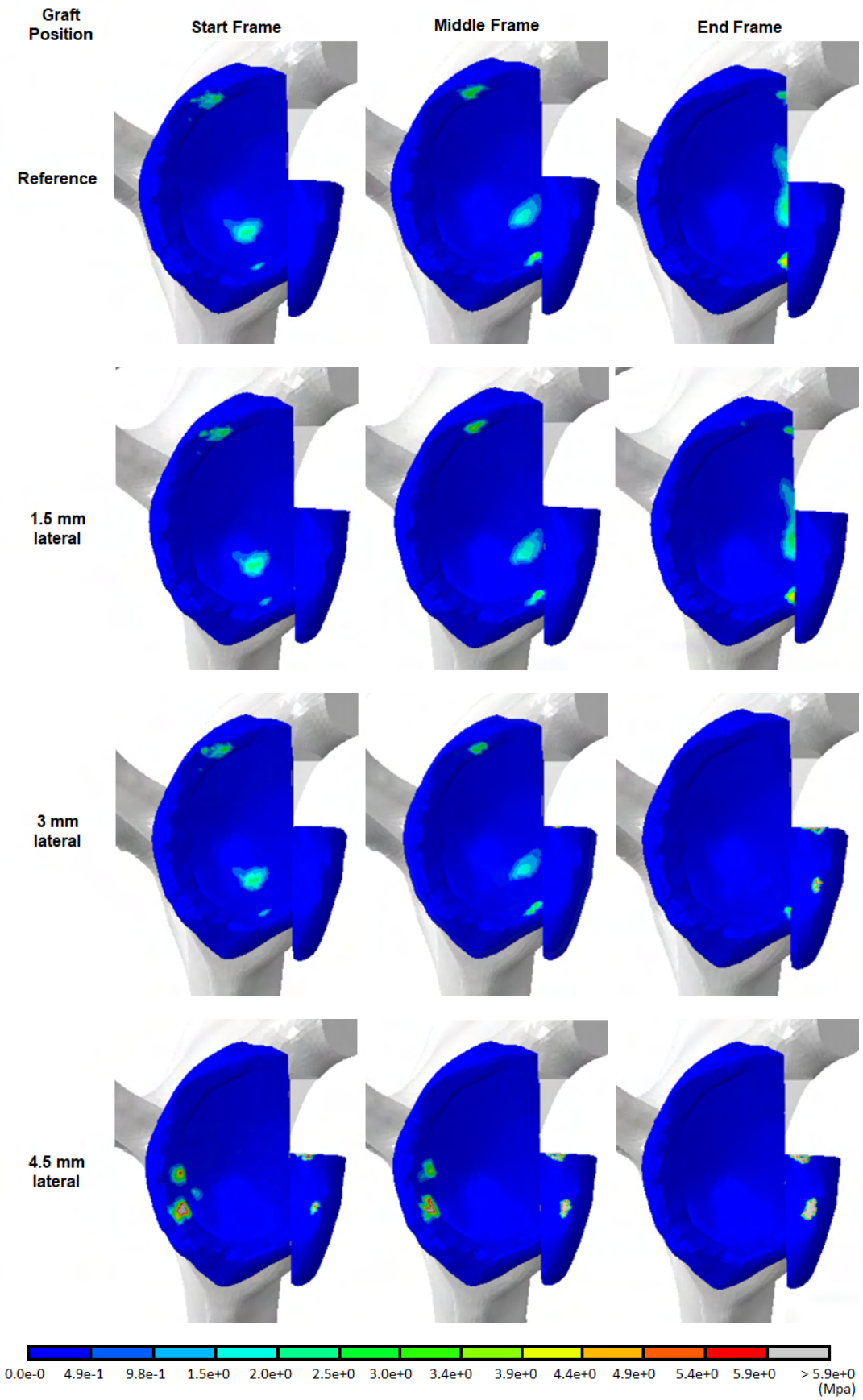

Figure A.3: Start, middle and end frames of the simulation showing contact pressure distribution on the glenoid cartilage, labrum and bone graft for each graft position at 60° abduction with 45° external rotation.

Appendix B

Mean Contact Pressure

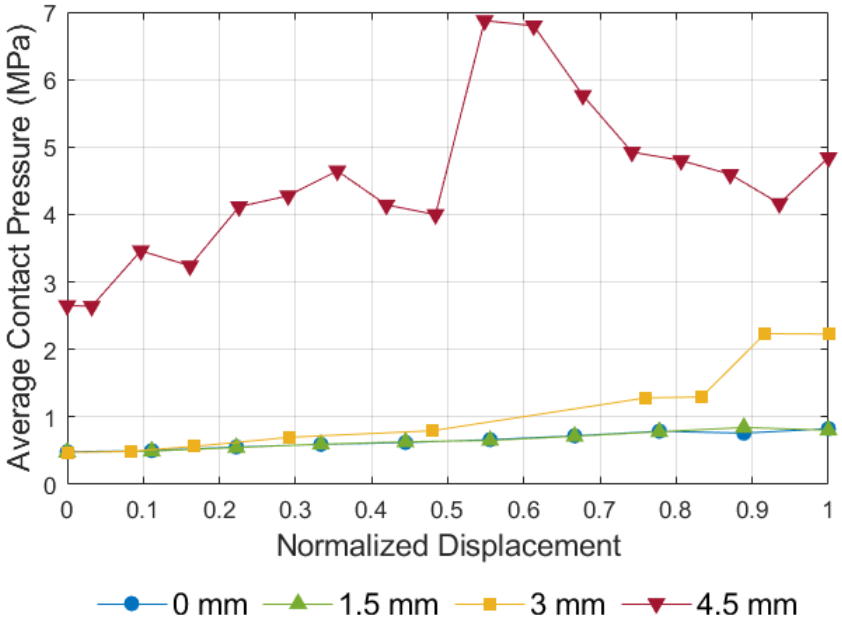

Figure B.1: Evolution of mean contact pressure with normalized displacement of the humeral head for the different graft positions at the neutral position.

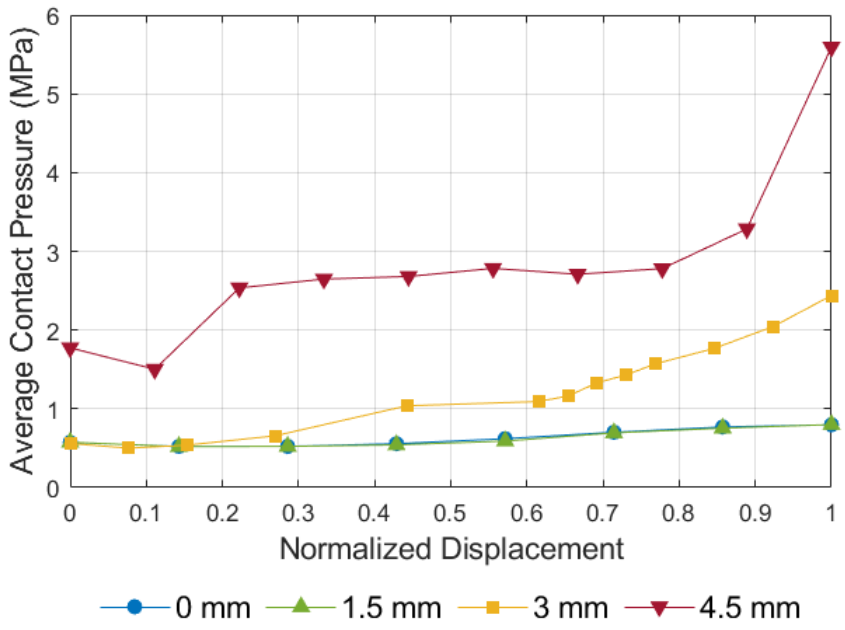

Figure B.2: Evolution of mean contact pressure with normalized displacement of the humeral head for the different graft positions at 30° GH abduction.

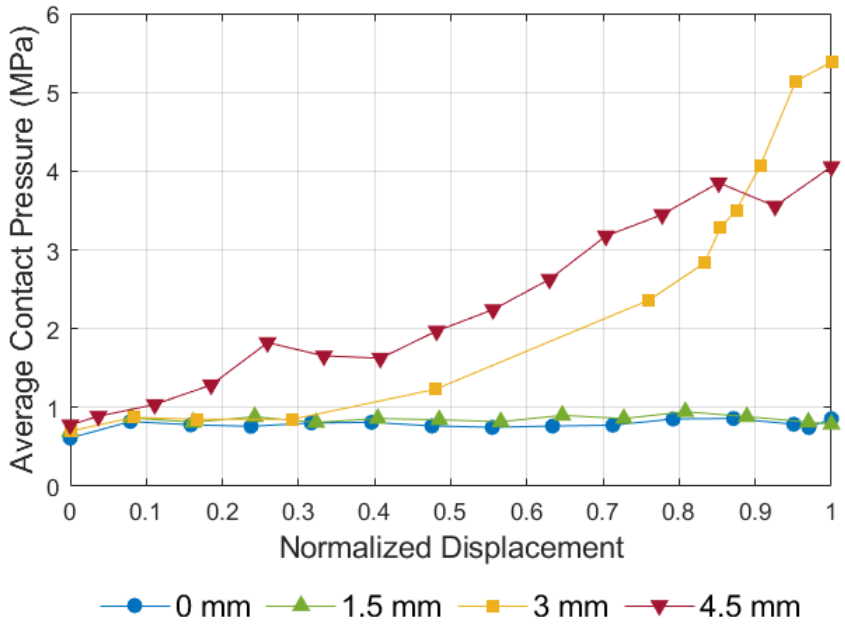

Figure B.3: Evolution of mean contact pressure with normalized displacement of the humeral head for the different graft positions at 60° GH abduction with 45° external rotation.

Appendix C

Contact Area

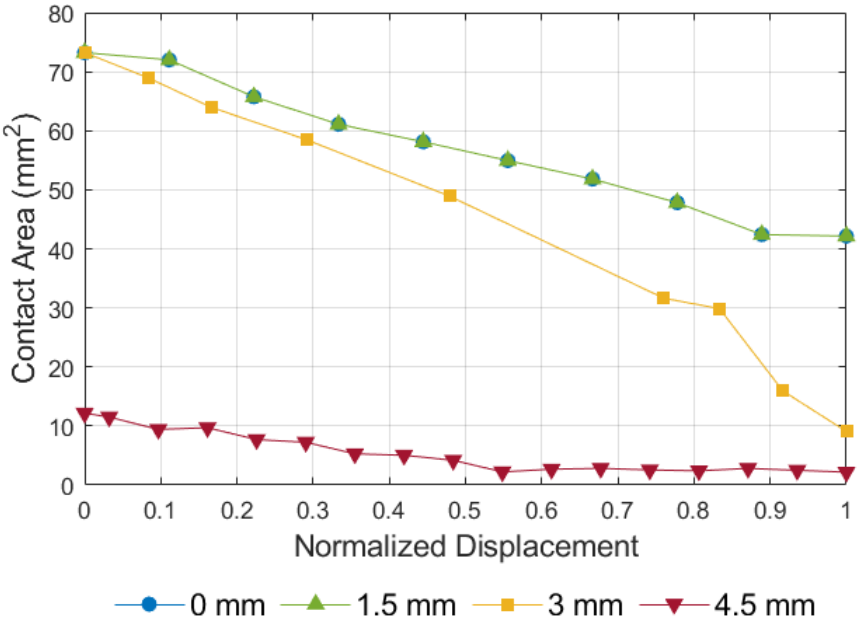

Figure C.1: Evolution of GH contact area with normalized displacement of the humeral head for the different graft positions at the neutral position.

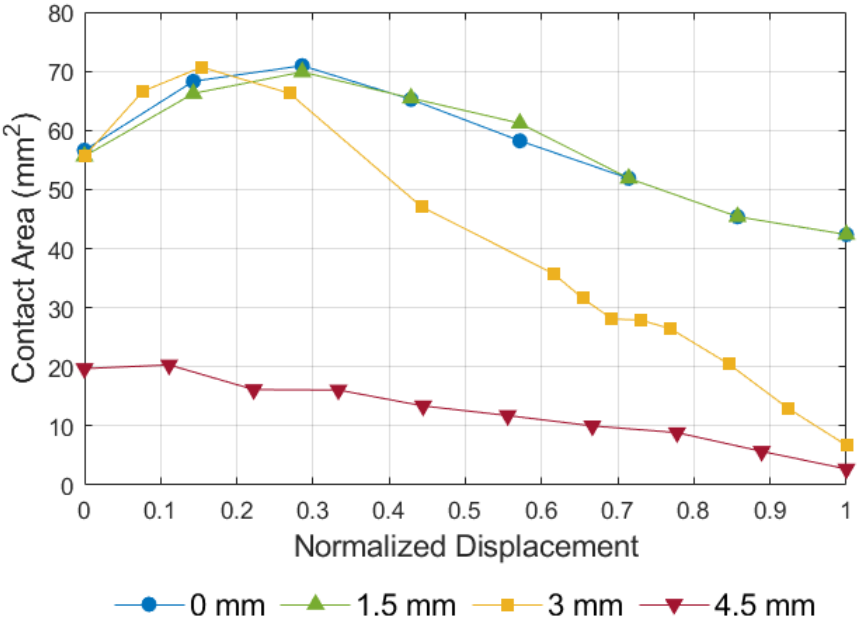

Figure C.2: Evolution of GH contact area with normalized displacement of the humeral head for the different graft positions at 30° GH abduction.

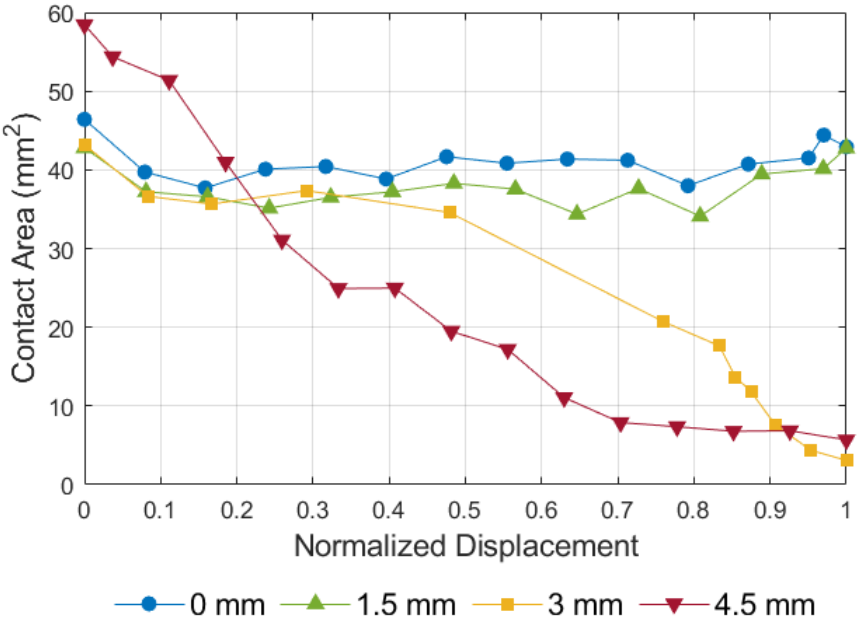

Figure C.3: Evolution of GH contact area with normalized displacement of the humeral head for the different graft positions at 60° GH abduction with 45° external rotation.